TÉCNICO LISBOA

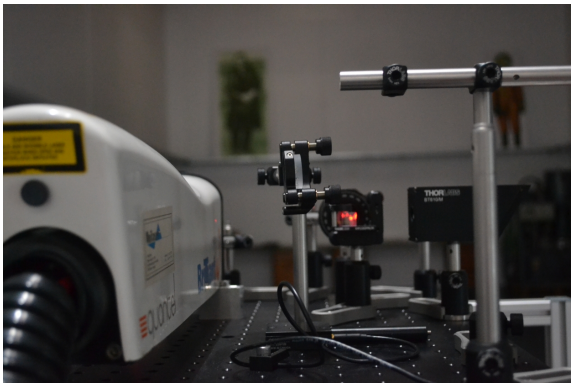

Laser Ignition of a High-pressure H_2/He/O_2 combustible mixture

Ricardo João Grosso Marques Ferreira

Thesis to obtain the Master of Science Degree in

Engineering Physics

Supervisor(s): Prof. Mário António Prazeres Lino da Silva
Prof. José António Sequeira de Figueiredo Rodrigues

Examination Committee

Chairperson: Prof. Horácio João Matos Fernandes
Supervisor: Prof. Mário António Prazeres Lino da Silva
Member of the Committee: Prof. João Alberto dos Santos Mendanha Dias

November 2017

Dedicated to my family and friends.

“If everything seems under control, you’re just not going fast enough.”
-Mario Andretti

“Really, you should always discuss the defeats because
you can learn much more from failure than from success.”
-Niki Lauda

“It’s equivalent if you take ten and then you give ten back. But if you take ten,
and then add something of yourself, you return eleven.”
-Alphonse Elric in *Fullmetal Alchemist*

Acknowledgments

Every year a new Formula 1 world driver's champion is crowned, and there can only be One. Nonetheless, each individual driver is supported by a massive team, from engineers, mechanics to trainers and a team leader. This master thesis may have my name in the cover but does not reflected all the people behind it, for who I own many thanks. First and foremost a thanks to our "team leader" and supervisor Prof. Mário Lino da Silva, that with help from Prof. José António Rodrigues and Dr. Maria Castela created this great learning and working opportunity. The ESTHER project could not be assembled and functional without the work of Prof. Bernardo Brotas de Carvalho and the Chief Engineer for the Hypersonic Plasmas Laboratory: Dr. Rafael Rodrigues. A second thanks to the Clean Combustion Research Center at King Abdullah University of Science and Technology for the welcome and the help in assembling the second experimental setup, in particular to professors Deanna Lacoste and Thibault Guiberti.

Even with all this people I could not be here if it were not for my friends and family. A driver is not complete without its fan club, neither am I without these people. My mother has a special place in this, not only for her encouragement for me to follow the dream of becoming a physicist, but also for her home made soup tupperwares and food which I warmed up every day through out five years. Similar to my mother, my father also was part of this great journey to become a Master in Physics, not only for his effort and dedication in bringing me everything I needed. Without my father how could I discover Formula 1 and being here making this silly, yet valid metaphore.

Of course this journey started many years ago, with the help of many professors and friends. I would like to thank in particular two of my Physics teachers, Zé Manel and Miss Té. Also to several friends "Trolhas do MEFT em Ação", "O Gabinete" and friends from my first course, Mechanical Engineering, with whom many study and work nights ended up be excitingly fun.

Resumo

A ignição a laser é um método promissor para inflamar misturas combustíveis a alta pressão. Consiste em focar um impulso laser de nanossegundos numa pequena região de modo a criar uma faísca elétrica e inflamar a mistura. Aquando da realização dos testes para o tubo de choque ESTHER, a equipa observou que um feixe laser desfocado poderia inflamar a mistura com pressões de enchimento entre 30-40 e 100 bar. A irradiância nessas condições é de aproximadamente 10^8 W/cm^2, 3 ordens de grandeza inferiores à irradiância média de outros estudos experimentais. Proposemo-nos a estudar o mecanismo pelo qual o gás absorve a energia do laser neste regime de alta pressão. Este revelou ser $< 5\%$ de energia total do laser. Os dados obtidos suportam a teoria de que a disrupção é criada devido a eletrões "de semente". A ignição seria devida à rápida ionização de partículas de poeira voláteis presentes na mistura, que excitam as moléculas de H_2 formando radicais altamente reativos e iniciando reações em cadeia. Outra experiência foi montada no Clean Combustion Research Center na KAUST, onde se mediu a energia de impulso mínima para inflamar misturas H_2-Ar à pressão atmosférica. Os resultados mostram uma energia de impulso mais baixa para a mistura estequiométrica, assim como dificuldades em inflamar a mistura perto do limite pobre.

Palavras-chave: Laser, Ignição, ESTHER, Alta Pressão, Hidrogénio

Abstract

Laser ignition is a promising method to ignite high pressure combustible mixtures. It consists on focusing a nanosecond laser pulse into a small size spot creating an electrical spark and thus igniting the mixture. When performing tests for the ESTHER shocktube development, the research team found that an unfocused laser beam could ignite mixtures with filling pressures of 30-40 to 100 bar. The irradiance in these conditions was about 10^8 W/cm^2, three orders of magnitude lower from the average irradiances reported in other experimental studies. We set to study whether the gas significantly absorbs the laser radiation in this high pressure regime. Less than 5% of the total laser energy was found to be absorbed, which supports the theory of seed electrons providing breakdown in laser-induced spark ignition. Ignition would then be achieved through the rapid ionization of volatile dust particles present in the mixture, which excite the H_2 molecules forming highly reactive radicals and start the chain reactions. Further experiment has been carried out in Clean Combustion Research Center at KAUST measuring the minimum pulse energy for H_2-Air mixture at atmospheric pressure. Lower pulse energies are required for igniting stoichiometric mixtures. There are difficulties in igniting mixtures close to the lean limit.

Keywords: Laser, Ignition, ESTHER, High Pressure, Hydrogen

Contents

List of Tables

List of Figures

List of Symbols

Greek symbols

α	Absorption coefficient
β	Microscopic absorption coefficient
γ	Heat capacity ratio
Δt_{pulse}	Laser's pulse time duration
Δ	Combustible mixture dilution
δ	Flame thickness
ε_i	Ionization energy
λ	Air:fuel equivalence ratio
λ_0	Laser's wavelength
ν	Frequency
ϕ	Fuel:Air equivalence ratio
ρ	Mass density
σ	Cross-section
τ	Chemical induction time

Roman symbols

c	Light velocity in vacuum
C_p	Heat capacity at constant pressure
c_s	Sound velocity
$\vec{E}$	Electric Field
E	Energy
E_f	Minimum initiation energy for the deflagration mode

E_g Minimum initiation energy for the detonation mode

f Lens focal length

I Irradiance

k Thermal conductivity coefficient

K_a Inverse Bremsstrahlung absorption coefficient

l Optical path length

n_e Electronic density

n_i Ionic density

P Power

p Pressure

$\dot{Q}$ Flow

Q Calorific Energy (Heat)

R Ideal gas constant

S_L Laminar Flame Speed

$\mathcal{T}$ Transmittance

T Temperature

t Time

w Laser beam radius

x, y, z Cartesian components

Subscripts

d Detonation mode

f Deflagration mode

List of Acronyms

CCRC *Clean Combustion Research Center*, research unit situated in KAUST.

ESTHER *European Shock-Tube for High Entalphy Research*, kinetic shock-tube being developed at Instituto Superior Técnico under funding from the European Space Agency.

FWHM *Full-width at half maximum*, the extent in the x-axis of a Gaussian profile at half it maximum height.

IB *Inverse Bremsstrahlung*, process through which free electrons absorb the laser energy and increase their kinetic energy.

KAUST *King Abdullah University of Science and Technology*, University in Saudi Arabia.

MIE *Minimum ignition energy*, the amount of energy sufficient to ignite a combustible mixture, function of parameters like pressure or temperature.

MPE *Minimum pulse energy*, minimum amount of the laser pulse energy needed to ignite a combustible mixture.

MPI *Multiphoton ionization*, mechanism for which a gas particle is ionization with the impact of several laser photons.

Chapter 1

Introduction

1.1 The ESTHER shock-tube

A new kinetic shock-tube for the support of Planetary exploration is currently being developed at Instituto Superior Técnico, under funding from the European Space Agency. This state-of-the-art facility, unique in Europe, will be used, for example, to design heat shields for spaceships, study the Kinetic processes of High Enthalpy plasmas, as well as others direct and indirect Plasma Physics topics. This kind of experimental facility, pioneer in Portugal, ushering a new age for Portuguese (and European) Space research as result of increased performance.

The requirements for the new ESTHER shock-tube (**E**uropean **S**hock-**T**ube for **H**igh **E**nthalpy **R**esearch) called for a facility operating beyond the current state-of-the-art. Three key aspects were emphasized: performance, repeatability, and availability. High performance implied a facility capable of producing shock-waves in excess of 10 km/s, repeatability implied being capable of reproducing the shock characteristics (essentially the shock-speed) with high precision, and availability mandated a design capable of low turnaround times and reasonable costs per shot. These required a simple yet efficient mechanical design. As such, they represented a challenge right from the conceptual design. The shock-tube has three main sections, the driver, an intermediary compression tube, and the test section. The last sections will not be discussed here since they go beyond the current objectives of the experimental work. The driver section was designed with a baseline operating pressure of 250 bar, with an option for high-performance operations at 600 bar. This is what drives the design. The driver is a piston-free combustion chamber designed for high-pressure deflagration of H_2/He/O_2 gas mixtures.

When considering a combustion-driven section, two different combustion modes have to be taken in to account. The first one is the traditional deflagration mode where combustion proceeds subsonically through heat and mass diffusion, with a smooth increase in pressure up until all the reactants have been burned. The second one is the detonation regime where combustion proceeds supersonically with a very steep and intense rise in pressure that ignites the mixture ahead of the wave, leading to a much higher peak pressure than the deflagration regime. The advantage of the detonation regime is a higher driver pressure but, it has the drawback of a lower shock repeatability, due to the inherent instability of

the detonation regime. This regime also imposes a increased stress levels on the containing vessel.

To create fast shock speeds very high-pressures are required in the driver section of the shock-tube - or more rigorously, a high ratio between the driver and driven section pressures (p_4/p_1) -, but it is also advantageous to achieve a high ratio between the corresponding gas sound speeds (c_{s4}/c_{s1}). As a result of this, a hot and low density gas is required in the driver section, leading to the choice of molecular hydrogen (H_2) as the most favourable combustible choice. The ignition of a pure H_2/O_2 mixture leads to detonation for H_2 molar fractions higher than 20%, therefore a inert gas dilution is necessary. The choice was He, since it is a noble gas (inert for most reactions) and has a low molar mass, therefore keeping a low mixture molar mass.

In order to design and size the preliminary driver section a considerable inspiration from the Convair combustion shock-tube developed in late 50's (in [1]), was taken into account. Further, to minimize the risks in designing and manufacturing such a large device, a scale model was built, a so-called "Bomb". This scale model of the combustion chamber allowed testing the ignition system, the gas filling system, the pressure measurement setup, and evaluate its mechanical behaviour. Even though this is a prototype, important results were obtained for gas filling pressures up to 100 bar, where as most H_2 combustion experiments in the literature rarely exceed filling pressures of 10 bar. There are notable exceptions, such as a series of experiments where done in Princeton up to 60 bar, Ref. [1], and in the Indian Institute of Technology Kanpur up to 30 bar, Ref. [2], for testing a laser ignition system. Figure 1.1 pictures a full-view of the ESTHER shock-tube, with the driver section on the left side.

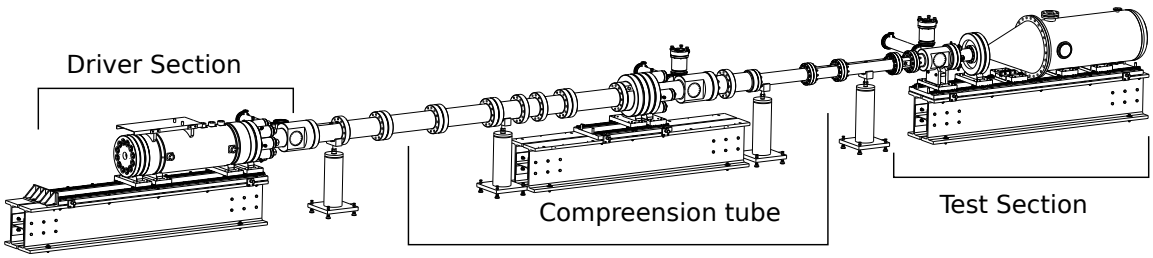

Figure 1.1: View of the ESTHER shock-tube, in [1].

1.2 ESTHER Ignition

The ESTHER test bombe has been designed by the Université de Provence, with an internal diameter of 80 mm, an external diameter of 240 mm, and a length of 600 mm, for a total volume of 3 l. There is an inlet and an outlet gas port, two ports for the hotwire system, one port for the pressure gauge, and two additional blanked ports. The maintenance access is through one of the end caps, since the other is connected to the outlet gas tube. Tightening is carried out using a star-shaped sequence with pre-tightening using a pneumatic tool, followed by a final torque using a manual dynamometric tool. Figure 1.2 shows a cutoff view and a picture of the "Bombe".

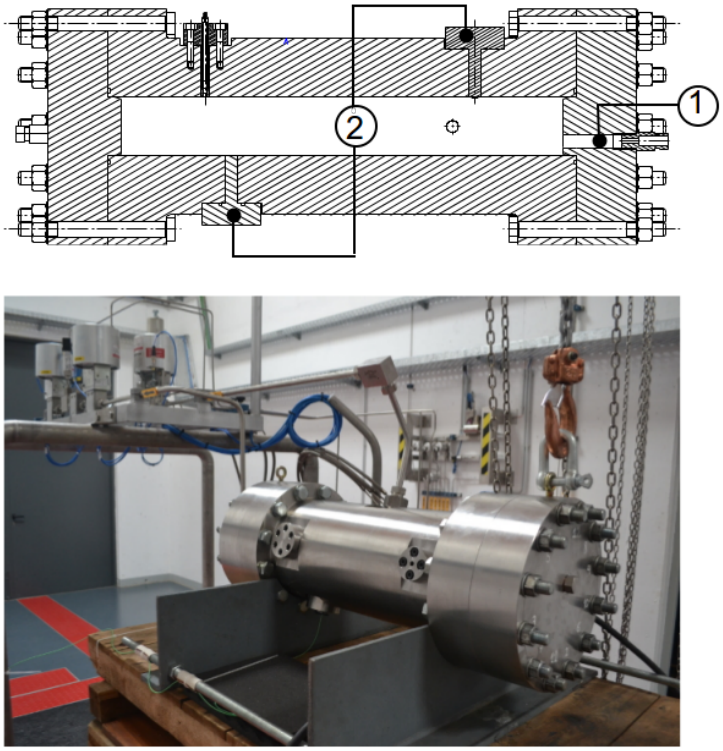

Figure 1.2: Outline design (top) and view of the Bombe and its associated gas filling system (bottom), in [1].

1 - Gas exhaust system; 2 - Constantan hotwire mounts.

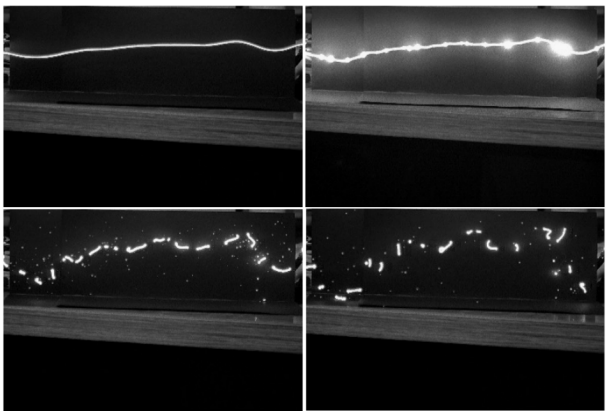

Figure 1.3: Fast video of a wire breakup experiment in inert air, Ref. [1].

Laser Ignition - Although a Constantan hotwire ignition system was first considered to ignite the gas mixture, it implied some drawbacks regarding simplicity and cleanness. Indeed, after each shot the chamber had to be cleaned and a new wire was needed, since it evaporates and/or pulverises as the gas ignites, as observed in Figure 1.3.

Although consumables & replacement parts cost is one of the drawbacks of the wire system, there are two other limitations which are more important: the first is the tendency for the Constantan wire to break or fall from the holder, depicted in Fig. 1.4, while in the preparation for an experimental shot. This not only leads to decrease the availability of the ESTHER, as it takes time to cut and place another

wire but, it also can be expensive in the case the chamber is already sealed and ready for ignition as the gases are extracted and cannot be reused. The second problem is associated with the wire itself, as it pulverises the pressure gradient pushes the particles towards the walls, at temperatures of around T=2500-2800 K, embedding the particles into the “Bombe” walls. As shots are being made, these particles accreted to the wall becoming a source of impurities in the system. Another problem is the accumulation of wire residues in the pressure sensor, shown in Fig. 1.5. This is critical for data acquisition since it is the only detector in the chamber.

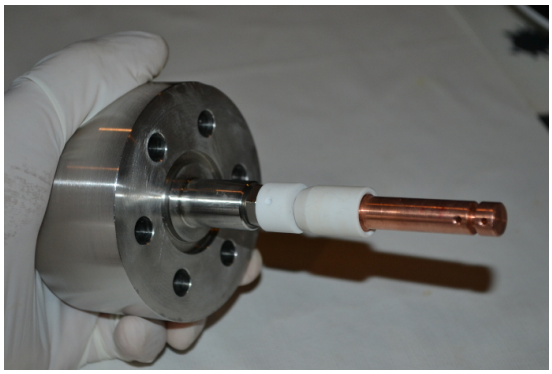

(a) Constant wire holder mounted before use.

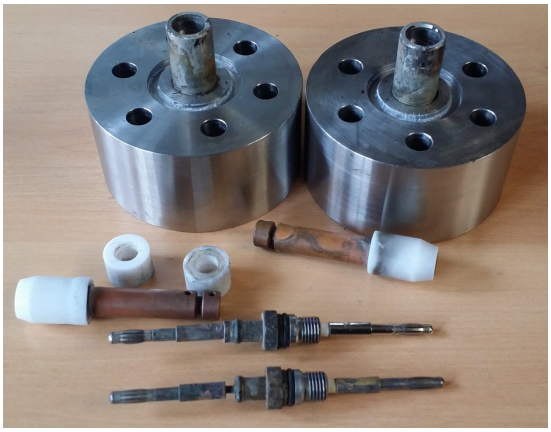

(b) Constantan wire holders pieces, note the wear in the plastic (white) piece.

Figure 1.4: Hotwire ignition system mounts.

With these problems in mind, a natural solution for ignition was to use a laser beam, described in detail in the Section “Experimental Setup” of this manuscript. The use of a laser required some minor modifications in the equipment and experimental setup. The first, and most obvious, was the manufacture of a window in the combustion chamber so that the laser can enter and interact with the mixture. The major difference, from an engineering point of view, is the mechanical stress applied to the window are, but the design minimizes this issue with increased safety margins regarding window’s thickness.

Figure 1.5: Pressure sensor for the test Bombe cover in Constantan dust.

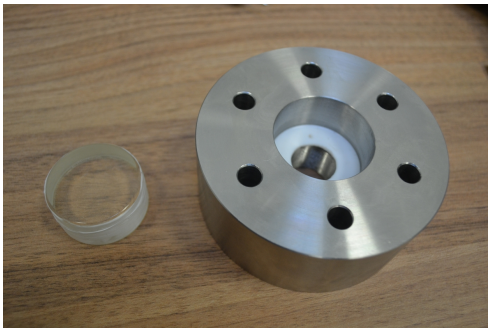

Figure 1.6: Laser window for the test Bombe, fused-silica round-window (left), support and chamber lid (right).

Several experiments were conducted in the combustion chamber to test all the different systems composing ESTHER project. For the laser ignition system related bibliography always referred the use

of a focusing lens, decreasing the laser spot size to increase the irradiance[1]. An interesting question, and incidentally the main motivation for this thesis, arose from successful a ignition[2] without focusing lens, subject not mention in the literature. The difference between a ignition reached through using or using not a convergent lens is exemplified in Fig. 1.7. The process was repeated coherently throughout the experimental campaign, proving it was not fortuitous, but a consistent physical phenomenon. This phenomenon was not understood and motivate us to research and try to comprehend the reason and the mechanism behind it. Figure 1.8 shows a schematic representation of both considered configurations.

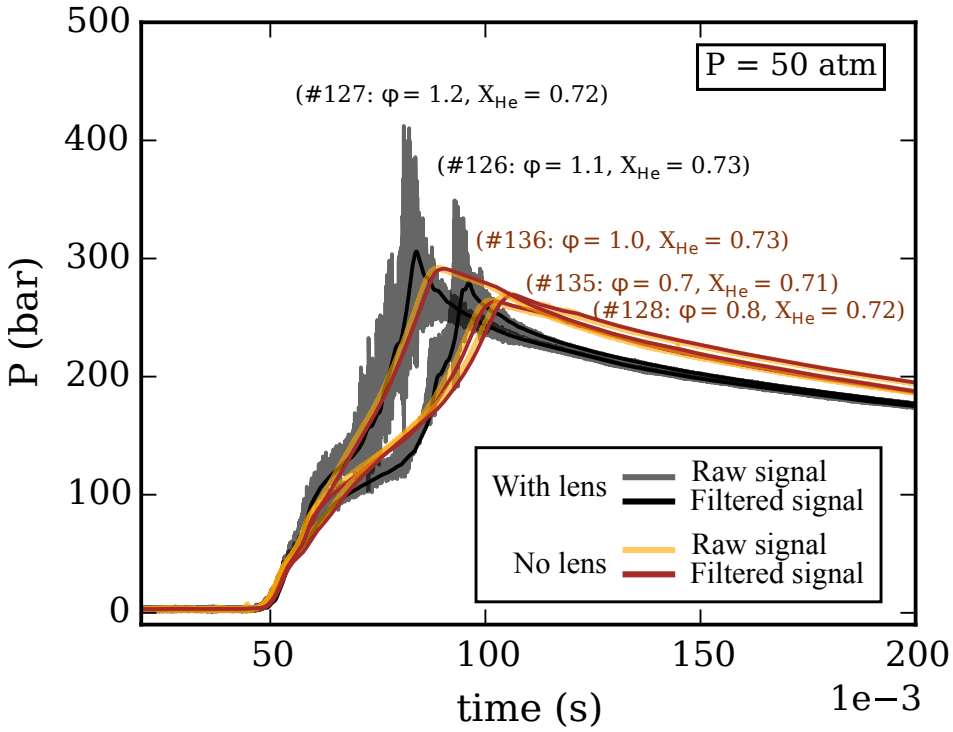

Figure 1.7: Pressure $vs.$ time of the combustion chamber ignited with both focused and non-focused laser beam.

[1] this will be discussed in detail ahead
[2] from filling pressure equal or higher than 20 bar

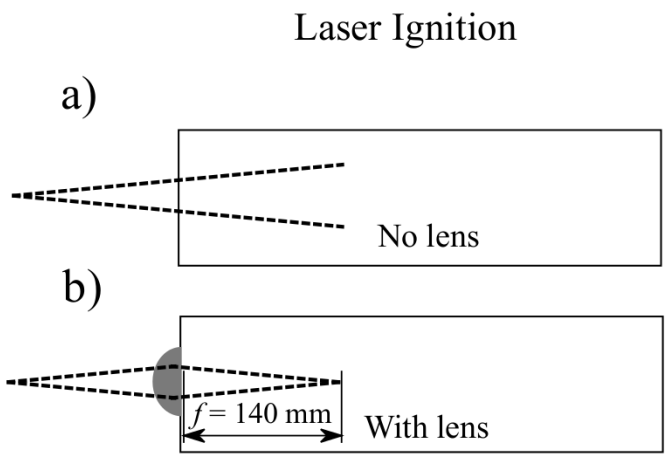

Figure 1.8: Schematic representation of the two different laser setup cases on ESTHER driven section. a) - Without focusing lens ; b) - With focusing lens, focal length $f = 140\mathrm{mm}$.

The ESTHER research team collaborate with the Clean Combustion Research Center, in King Abdullah University of Science and Technology, to further study laser ignition in hydrogen mixtures. With this, we created the opportunity to study laser ignition in H_2-Air mixtures at atmospheric pressure, a set of conditions not possible in the ESTHER setup. This collaboration provided not only experimental advantages, as a new setup could be assemble, but also an exchange of scientific ideas and hypothesises in laser ignition phenomena.

1.3 Objectives

The objectives of this work are:

(1) Identification of the mechanism through which the laser energy is transferred to the gas mixture

(2) Understanding the impact of laser optical configuration on the mixture ignition at high pressures

(3) Obtaining the minimum pulse energy to ignite H_2-Air mixtures at atmospheric pressure

This work aimed at contributing to the future design of an effective laser ignition systems for both practical and academic applications. Namely, the mechanism mentioned in point 1 is relevant not only for practical reasons, but also for analytical modelling of laser-gas interaction.

1.4 Thesis Outline

This thesis is composed of 5 chapters, of which the current is the Introduction. Chapter 2 is a review of the State-of-the-Art. Chapter 3 presents the experimental setup and procedure of the performed experiments, followed by the presentation and discussion of these results in Chapter 4. Lastly, the main conclusions and suggestions for future works are in Chapter 5.

Chapter 2

State-of-the-Art

As a way of using energy in practical applications, combustion is one the first scientific achievements. It is an important energy extraction method in today's world, as it is used to generate electricity, transportation in vehicles such as cars, airplanes, boats, to provide home heating and the list goes on. It is known that combustion has many advantages, since storing fuel is simple and fuel can have high energy density, meaning that a certain amount of gasoline, for example, can provide much more energy (chemical) than an electric battery of the same mass. The major disadvantages combustion presents are its thermal efficiency limit to produce mechanical work and the somehow toxic chemical emissions.

When a system transforms energy from a form to another, let's say chemical to mechanic, energy losses can occur. These energy losses can be derived from the construction/manufacturing itself, which has drag, imperfections, as it is not a pure theoretical exercise. Besides that, a thermal engine has inherent power losses, since not all its thermal energy can be transformed into mechanical work. For a practical application there are even more power losses, being a simple example a combustion where not all the fuel is totally burned, an incomplete reaction. Any amount of unburned fuel is clearly an energy losses, and decreases the system efficiency.

It is known that combustion releases gases as products of its chemical reaction, these gases can be pollutant such as carbon dioxide or nitrogen oxides. Minimizing pollutant emissions and maximizing efficiency are the new set of challenges presented to combustion science and engineering. For a combustion reaction to occur there are needed three key ingredients: a fuel to burn, or rather oxidise, an oxidizer and a ignition source to start the chemical reactions. This is illustrated in Fig.2.1, and any missing element stops the reaction.

Figure 2.1: Combustion triangle

A typical combustion reaction uses oxygen, O_2, to react with the fuel. Two important parameters are defined in relation to the amount of different chemical species before reaction: the pre-mixture's air:fuel equivalence ratio λ and the dilution Δ. The first parameter is defined as the ratio between the number of molecules n_{air} of air (or oxidizer in a more general way) to fuel n_{fuel}, normalized to the stoichiometric coefficients of the reaction. The latter is defined as the fraction of inert species n_{iner} in the pre-mixture, both mathematically defined in Eq. (2.1).

$$\lambda = \frac{n_{air}}{n_{fuel}} \Bigg/ \left(\frac{n_{air}}{n_{fuel}}\right)_{stoi} \qquad \Delta = \frac{n_{iner}}{\sum_{j=1}^{k} n_j} \quad . \tag{2.1}$$

The stoichiometric reaction occurs when there is no excess of either fuel or oxygen. Taking hydrogen as fuel, for example, and α, β, γ numerical coefficients, to balance this reaction so the number of atoms of each species in the reactants, in the left-hand side, and products, in the right-hand side, α, β, γ should be 2, 1, 2, respectively. So the air:fuel equivalence ratio in stoichiometric conditions is 1.

$$\alpha H_2 + \beta O_2 \rightarrow \gamma H_2O$$

Two regimes of pre-mixtures are defined as function of λ. The first is called "rich", when $\lambda < 1$, the other "lean" when $\lambda > 1$. Finally the ignition is what starts the reaction, it can be done using an electric discharge of a spark-plug, a laser or by heating the pre-mixture, among others. The idea is to overcome the chemical potential of the reactive species, even if only locally, so they can react and release more energy, which starts the chain-reaction leading to full scale combustion. The flame front is the region between the burned and unburned fuel, which starts at the ignition point and expands outwards. As

the flame grows and energy is released the temperature, and subsequently the pressure, rise. This pressure rising is used to generate mechanical work in a turbine or piston, for example, in a so called internal combustion engine.

When considering the flame propagation two different combustion modes have to be taken into account. The first one is the traditional deflagration mode where combustion proceeds sub-sonically through heat and mass diffusion, with a smooth increase in pressure until all the reactants have been burned. The second one is the detonation mode where combustion proceeds supersonically with a very steep and intense rise in pressure that ignites the mixture ahead of the wave, leading to a much higher peak pressure than the deflagration regime. The conditions for the combustion modes depend on the geometry of the combustion vessel, ignition source, initial pressure, homogeneity, air:fuel equivalence ratio and dilution of the pre-mixture. Higher pressures and small dilutions tend to originate detonations, since there are no inert species to absorb the excess energy. The air:fuel equivalence ratio dependence is not monotonous as it depends on thermal diffusivity of the mixture and different fuels have different diffusivities.

2.1 Ignition Phenomena

2.1.1 Phenomenological Description

Ignition in premixed gases was described by Lewis and Elbe [3], and citing: "If a subcritical quantity of energy in the form of heat and/or radicals (chemically active atoms or molecules) is deposited on a combustible mixture, the resulting flame kernel decays rapidly because heat and radicals are conducted away from the surface of the kernel and dissociated species recombine faster than they are regenerated by chemical reaction in the volume of the kernel. The kernel extinguishes after consuming a small quantity of reactant. On the other hand, if the ignition energy exceeds a certain threshold [called the *minimum ignition energy* (E_f)], at the time when the peak temperature decays to the adiabatic flame temperature T_f, the temperature gradient in the kernel is sufficiently shallow that heat is generated in the kernel faster than it is lost due to conduction to the unburned mixture. This leads to the development of a steady flame that consumes all of the available mixture. This description indicates that ignition is in general characterized by an minimum total energy rather than a minimum temperature or energy density."

It may look incompatible with the the computational calculations of Maas [4] where they report the energy density to be the crucial condition. Despite this, both descriptions are not antagonistic. Maas, in [4], fixed all the parameters except the energy and the ignition source size to conclude that, for a big enough ignition source energy density was the crucial parameter and this can be seen as the existence of a critical gradient related to the balance between gain and loss processes and a minimum flame kernel radius requirement. For a planar flame, this balance leads to the definition of flame thickness δ_f, a characteristic size. Therefore, the most simple physically realistic ignition criteria is that E_f must be enough to increase to T_f the temperature of a gas sphere with radius δ_f. Both δ_f and E_f are function

not only of the combustible mixture, but of the ignition source as well. A typical value for a stoichiometric H_2-air mixture is 0.002 mJ.

When considering the detonation mode the characteristic propagation rates are too high for heat conduction to be and important factor, therefore the previous model is not applicable. Identifying a minimum ignition energy for detonation E_d is more difficult since it can be initiated directly or indirectly. The indirect method starts with a deflagration, which subsequently accelerates to a detonation front through the interaction and gas-dynamic amplification of pressure waves, reflected off nearby walls, pressure-pilling, with the evolving front. This method greatly facilitates detonations since $E_d \gg E_f$, as will be discussed in the following paragraphs.

Direct initiation of detonations require a minimum ignition energy E_d because the temperature rise in the mixture behind the shock does not lead to an instantaneous heat release to sustain the shock. A chemical induction time τ_d must elapse before the chemical reaction's heat release is complete. In an analogous form, if the shock decays in strength before it can be replenished by the released heat the detonation wave will disappear, but it can also relax to a deflagration. Hence, a detonation wave has a characteristic thickness $\delta_d \sim u_d \tau_d$, where u_d is the velocity of the gases behind the leading shockwave. Combustion theory demonstrate that burning gases at the local sound speed c_s are the only stable detonations, the so-called Chapman-Jouget detonation. Using a criteria similar to the deflagration mode, E_d must rise a sphere of radius δ_d to the product temperature T_d and pressure p_d.

2.1.2 Minimum Ignition Energy

Deflagration mode

To estimate the minimum ignition energy on deflagrations one can use a thermal hypothesis. Following this, E_f and δ_f can be estimate relating it with the gas thermal characteristics, thermal conductivity, k, heat capacity at constant pressure, C_p, and flame speed, S_L. Flame kernel is estimated by:

$$\delta_f \approx \frac{\overline{k}}{\rho_0 C_p S_L} = \frac{\overline{k}}{k_0}\frac{\alpha_0}{S_L} \quad \text{and} \quad \alpha_0 \equiv \frac{k_0}{\rho_0 C_p}, \tag{2.2}$$

where the overbar denotes an averaging over temperature. One can similarly estimate a characteristic deflagration time $\tau_f \approx \delta_f / S_L$. Therefore the enthalpy in a sphere of radius δ_f, which is presumed to be E_f, where Q is the heat, is given,

$$\begin{aligned} E_f &\approx \frac{4\pi}{3}\delta_f^3 \rho_f Q \approx \frac{4\pi}{3}\left(\frac{\alpha_0}{S_L}\right)^3 \rho_f Q \left(\frac{\overline{k}}{k_0}\right)^3 \quad , \\ Q &\equiv C_p(T_f - T_0) \quad . \end{aligned} \tag{2.3}$$

A more precise description of flame ignition include the effects of Lewis number (Le), which is defined as the ratio of thermal to the mass diffusivities. In most combustible mixtures Le is close to the unity, so the above estimative is correct.

Detonation mode

Using a similar approach for detonations to the one used for deflagration, and setting the fluid velocity approximated to the local sonic speed leads to the rough estimative of the minimum ignition detonation to be:

$$E_d \approx \frac{4\pi}{3}(c_s\tau_d)^3\rho_d Q \quad . \tag{2.4}$$

A more accurate estimative considers the ignition source as an expanding spherical shock front. The crucial condition is that the pressure behind the shock is equal or larger than p_d when it reaches the radius $c_d\tau_d$. This leads to

$$E_d \approx \frac{125\pi J}{2}\rho_0\tau_d^3(c_0 M_{cj})^5 \quad , \tag{2.5}$$

where J=0.423 for a spherical detonation in a mixture with heat capacity ratio γ=1.4, and M_{CJ} is the Mach number of the Chapman-Jouget detonation in relation to the unburned gas,

$$M_{CJ} \approx \left[1+\frac{q(\gamma^2-1)}{2\gamma}\right]^{1/2} + \left[\frac{q(\gamma^2-1)}{2\gamma}\right]^{1/2} \quad , \tag{2.6}$$

where $q \equiv Q/RT_0$, with R the ideal gas constant. Typical values for q and γ at stoichiometric conditions yields $M_{CJ} \approx 7$. Comparing the minimum ignition energies for both regimes through Eqs. 2.3 and 2.5 results in:

$$\frac{E_d}{E_f} \approx 8\left(\frac{c_0}{S_L}\right)^3\left(\frac{\tau_d}{\tau_f}\right)^3 M_{cj}^5 \quad . \tag{2.7}$$

Since the sound speed is much greater than the laminar flame velocity and the characteristic times are roughly of the same order of magnitude, it is trivial to conclude that $E_d \gg E_f$. For example, in stoichiometric H_2-O_2 mixture at 1 atm E_d it about 10 J, while E_f is 1 μJ.

Main differences on minimum ignition energies

Minimum ignition energy can be influence by the following parameters:

• Gas mixture composition - Several studies have determined the influence of the combustible mixture's composition in E_f or E_d, being the most studied effect the influence of air:fuel equivalence ratio, λ. The main effect of λ is on T_f or T_d, because of the highly-temperature dependence of most combustion reactions and its effects on the timescales. Therefore, this effect influence the minimum ignition energies as Eqs. (2.3) and (2.5) predict $E_f \sim S_L^{-3}$ and $E_d \sim \tau_d^3$, respectively. Both predictions are consisting with experimental data presented by various authors, namely Ronney in [5].

• Ignition source size - Considering an optimum dimension for the ignition source, d_{opt}, e.g. the spark gap in an electric spark plug, for which E_f is minimized. Generally, E_f decreases rapidly up to d_{opt} and then increases slowly. When this gap distance, d, is larger than δ_d a larger volume of mixture is required

to be heated. For $d \gg d_{opt}$ we recover from Eq. (2.3) $E_f \sim d^3$. In the opposite direction, the temperature gradient are higher increasing radiative losses. Besides that, smaller volumes implies the formation of stronger shock waves that carry away energy out of the ignition region.

• Duration of energy deposition - Similar to source ignition, time t has an optimum value for which E_f is minimum. If the deposition time is large enough, the flame starts to propagate away from the ignition source before all of the energy is deposited, increasing E_f, in an identical form to d, for much greater times t than the optimum $E_f \sim t$. If the deposition is to fast, it is thought that higher kernel temperatures are achieve, which translate in greater radiative losses, or shock wave formation. This last point is of particular interest for laser ignition, where t is of the order of nanoseconds or picoseconds, leading to the formation of shock waves. Although, if the shock wave decays to weak pressure waves at radius less than δ_f, the energy less is minimal.

• Gas mixture flow - Ballal and Lefebvre in [6] did experiments on the effects of flow velocity, u, in relation to the spark electrodes. It was concluded that E_f increases with increasing u, however, it is required $u \gg S_L$ for significant effects to be observed. The reason to this increase is that due to aerodynamic straining that expands the flame kernel area. Besides this, turbulence tends to also increase thermal diffusivity, which increases δ_f, thus increasing E_f. Studies of flow influence in detonation regimes were not found. Since the characteristic velocities for detonation are on the order of sound speed, this would imply supersonic flows so any effects in E_d could be observed.

2.2 Laser Ignition Theory

Laser is an emerging technology for the 21st century, with applications in Medicine, Biology, Chemistry and Mechanics, among other fields. Clearly the main field of laser application is Physics, starting from Fundamental up to Engineering or Experimental Research. Laser is the acronym for **L**ight **A**mplification by **S**timulated **E**mission of **R**adiation, first predicted by Albert Einstein with its principle of stimulated emission proposed in 1917. A laser is a light emission device capable of emitting coherent light. This means a laser is capable of emitting light waves of the same wavelength, phase and polarization, and can be focused into a tiny spot. Since the light emitted from a laser is coherent it is capable of deploying very short time pulses, and combining it with a small spot means a very high irradiance, which ahead will be explained. Today the laser is the light source most similar to a point-like source.

The first laser was produced in 1960 by Theodore H. Maiman at Hughes Research Laboratories, based on theoretical work by Charles Hard Townes and Arthur Leonard Schawlow. A laser is constituted by a gain medium, a mechanism to stimulate it such as a flash lamp, electric current or another laser, and an optic feedback element, such as a semi transparent mirror. The medium is stimulated and starts to emit light, which is then amplified by stimulated emission. This light bounces between two mirror/mirror-like surfaces and continues the process, increasing its power.

The gain medium is a material whose properties allow it to amplify light by way of stimulated emission, at a specific wavelength. This light bounces between two mirror or mirror-like surfaces, feedbacking the medium and increasing its power. Usually one of the mirror surfaces is semi-transparent to the

resonance wavelength, so the fraction of light that passes through is the output beam. A detailed mathematical formulation and physical description of a laser beam is presented in Appendix A. For our work the most important equations are the Beer-Lambert's law and laser's irradiance or intensity, taken from [7]. Beer-Lambert's law relates the power loss of a light beam as it travels through a medium with an absorption coefficient α,

$$P(x) = P_0 \exp(-\alpha \cdot l) = P_0 \cdot \mathcal{T} \quad , \tag{2.8}$$

where P is the power, l the optical length, P_0 the initial power and $\mathcal{T}$ the system's transmittance. If the total (initial) power, P_0, is given by the sum of transmitted power and absorbed power, $P_0 = P_{abs} + P_{trans}$, therefore from Eq. (2.8), P_{abs} is given by:

$$P_{abs} = (1 - \exp(-\alpha \cdot l))P_0 \quad . \tag{2.9}$$

It is clear from Eq. (2.9) that the deposited energy in the mixture only depends on the absorption coefficient, since the laser power and optical length are constants for a fixed setup.

The average irradiance I is the luminous energy per unit area per unit time. For a laser with pulse energy E_{pulse}, pulse duration Δt_{pulse}, defined as the *FWHM* (Full Width at Half Maximum of a Gaussian pulse), and beam diameter $2w$, its average irradiance is given by:

$$I = \frac{E_{pulse}}{\Delta t_{pulse}} \frac{1}{\pi w^2} \quad . \tag{2.10}$$

Laser ignition is a new and promising method to ignite gas and liquid combustible mixtures, either with or without liquid phase. Nowadays the commercial source of ignition in gas turbines and reciprocated engines (commonly known as piston engines) are manly electric spark-plugs. Laser ignition provides important advantages as technology looks for more efficient and less pollutant combustion devices. In order to achieve that, hydrogen is being researched as an alternative fuel to methane and other hydrocarbon based gases. Hydrogen has a very wide flammability range, meaning it can be ignited for λ between 0.2 and 5 within certain other parameters. Besides that, higher efficiency can be achieved using higher pressures and a leaner air:fuel equivalence ratio. Hydrogen burning appears to not produce pollutant gases since the theoretically chemical reaction in air, where oxygen is mixed with nitrogen, is expressed as

$$2\mathrm{H}_2 + (\mathrm{O}_2 + 3.76\mathrm{N}_2) \rightarrow 2\mathrm{H}_2\mathrm{O} + 3.76\mathrm{N}_2 \quad .$$

For what is depicted the nitrogen is non-reactive gas, only being part of the reaction since it is present in air. But in fact that is not true, the real reaction passes through various intermediate reactions, which can lead to the formation of other chemical species. A complete computational study of ignition of hydrogen-oxygen mixtures was performed by Maas and Warnatz in [4]. In their work they explore the formation and destruction of various chemical species during a pure hydrogen-oxygen burn. This intermediate species formation is also presented and explained in [8], and it is reasonably simple to

understand that nitrogen can react with oxygen to form nitric oxides. These nitric oxides are the only pollutant gases in hydrogen burning, and that is why it a so interesting fuel.

More extensive studies on λ's influence were made by Heffel and Shudo et al. in [9, 10], where they vary the air:fuel equivalence ratio and measure the NO_x emissions and efficiencies. The main reason is that lowering the amount of fuel decreases the flame temperature and makes the formation of NO more difficult, since this chemical process requires energy. Besides this, increasing the oxygen content implies that more of the total input fuel is burned in the chamber, therefore fewer energy losses occur.

To ignite a mixture, an ignition source is needed, as presented in Chapter 1. Maas and Warnataz in [4] also studied how the ignition source size and energy influence the ignition. Their simulations were made in a 2:1:10 hydrogen-oxygen-nitrogen mixture with an initial pressure of 1 bar and ignition time of 100 μs. They concluded that the energy needed to ignite is proportional to the ignition source size, for a sufficiently large source, meaning a constant energy density. If the ignition source is too small, diffusion and conduction losses occur and disperse the energy faster than the chemical reactions time. Higher pressures reduce the diffusion losses but increase the heat capacity, leading to faster heat losses. This means minimum ignition energy decreases with pressure up to a point were heat capacities start to domain and minimum ignition energy increases. In a practical analysis, this is also function of the ignition method, the spark-plug electrodes quench the heat, while the laser does not have this limitation, a case to case analysis is needed for better understanding.

For a conventional ignition system to work, increasing pressure implies a need to increase the voltage and energy between the electrodes. Despite that, ignitability, the probability of igniting a mixture for a fixed set of parameters, does not always improve, but it does create greater reliability problems. Typical problems include secondary high voltage breakdown, poor timing sensor reliability and electrode degradation. It is in this conditions that laser looks as a promising choice of ignition, whose main advantages are:

- Choice of arbitrary position and timing of ignition;
- Absence of quenching effects by the spark plug electrodes;
- Capability of ignite leaner mixtures, which release less NO_x;
- No erosion effect on the electrodes, meaning a longer system's lifetime;
- Exact regulation of the deposit energy;
- Easier multipoint ignition;
- Shorter ignition delay and shorter combustion time.

In order to achieve ignition with a laser the laser energy needs to be transferred to the combustible mixture, starting the chemical reactions leading to a full scale combustion. From a fundamental stand point, the laser energy can be transferred through four different methods, which are: a) Laser Thermal ignition; b) Laser-induced photochemical ignition; c) Laser-induced resonant breakdown ignition and d) Laser-induced spark ignition.

2.2.1 Laser thermal ignition

Thermal ignition utilizes the energy of the laser beam to increase the kinetic energy of the target molecules, in either translational, rotational, or vibrational form. This typically leads to a long ignition delay time. The laser can be used for point-like ignition or line-like ignition source. Despite this, point-like ignition is very difficult to obtain. This is due to the local energy deposition is approximately linear to the beam's intensity, so the region near the focus tends to heat and not only the focal point, as was pointed out by Ronney in [5]. To overcome this limitation, small targets inside the mixture can be heated by the laser, such as aluminium particles.

Since point-like thermal ignition is extremely difficult to obtain, most of the literature focus on homogeneous ignition. This type of ignition depends mostly on the thermal heating and gas dynamics of the mixture during the heating process as pointed in [11]. The authors of [12, 13], studied ignition of H_2-O_3 and H_2-O_2 on a cylindrical cell using a TEA CO_2 laser. They report the ignition occurred near the entrance window, and propagates in both radial and longitudinal directions thanks to inhomogeneous laser absorption. Continuous wave laser have also been studied since those avoid shockwaves generated by the sudden energy deposition.

Laser thermal ignition have important limitations. The primary limitation is that the mixture must have a strong absorption at the laser's wavelength. It is possible to use other gases such as SF_6, SiF_4, NH_3 or CH_3F to absorb the laser energy and then transmit it to the reactive species. Another limitation is when trying to use this mechanism as a line-like ignition source. During the induction period, the gas dynamics due to energy absorption and acoustic instabilities, derived by thermal expansion, change the ignition kernel geometry, therefore producing a line-like ignition source is extremely complicated. Nonetheless, this mechanism is used to ignite solid propellant in rockets (first igniting pyrotechnics) because contrary to gases, liquids, and solids in particular, absorb in the infrared spectrum.

2.2.2 Laser-induced photochemical ignition

Photochemical ignition is characterized by the formation of highly reactive species due to laser-molecule interactions. If the production rates are greater than the recombination ones, the usual chemical chain-branching reactions start, leading to a full-scale combustion. Lucas in [14] studied photochemical ignition of H_2-O_2 mixture using an KrF excimer laser at 248 nm. It was conclude that the energy density is not the crucial factor, but instead the concentration of radicals produced by the absorption of a single photon. It was reported that to ignite a mixture it is needed a minimal radical concentration of 1.2×10^{17} atoms/cm^3. This requirement was also reported in [15, 16], whose studies focus on H_2-O_2 and H_2-air using excimer laser at 157 nm and 193 nm. The initial absorbing species in these mixtures is molecular oxygen, which strongly absorbs in vacuum ultraviolet (VUV) region of 130-175 nm. The minimum oxygen atomic concentration to ignite was calculated as 3×10^{17} atoms/cm^3.

When comparing to thermal ignition the major difference is that the latter needs a minimum of energy and size are required. When comparing with the other mechanisms, photochemical ignition occur at lower pressures and closer to the flammability limits, as long as the minimum radical concentration is

obtained. This means that, due to its fine tuning, it is energetically very efficient.

Using photochemical ignition has several disadvantages in practical applications. A fine tuning is required between the laser wavelength and the molecules absorption wavelength in order to dissociate them. Besides this, most lasers work with visible or Near-Infrared radiation, while the dissociation energy is mostly on the UV. At present, UV lasers are expensive and complex while in practical applications compact, lightweight, cheap and robust lasers are required.

2.2.3 Laser-induced resonant breakdown ignition

Resonant breakdown is a two-step process, the first is partially similar to spark ignition and the second to photochemical ignition. Firstly, some of the molecules are dissociated through non-resonant multiphoton photodissociation, then followed by the resonant photoionization of the now dissociated atoms. This leads to the formation of seed electrons, which increase their energy by the inverse bremsstrahlung (IB) process to form a plasma, igniting the mixture. Forch and Miziolek in [17] proved that the plasma formation and ignition of H_2-O_2 and H_2-N_2O mixtures is due to this process. In their experiment, a tunable UV laser emitting laser pulses at 225.6 nm wavelength was used to produce atomic oxygen from two-photon dissociation of O_2 and N_2O. These atoms were then ionized with two/three-photon photodissociation. In a following experiment [18], the authors demonstrate that the same process is responsible for igniting deuterium-oxygen mixtures at atmospheric pressure, the difference being the laser wavelength (λ_0=243.7 nm for hydrogen and 243 nm for deuterium) used to cause gas breakdown. The authors, Forch and Miziolek, prove in their study that the ignition is carried out by the photolysis of hydrogen/deuterium atoms followed by resonance-enhance multiphoton ionization of the atoms. The resonant multiphoton process is supported by the spectral profile of emission signals from the laser-induced plasmas in H_2-O_2 mixtures. It was blue-shifted with respect to that of D_2-O_2 mixtures, in a nearly identical shift to the H-D isotope shift.

Due to the resonance ionization this process is extremely efficient when compared to non-resonant breakdown where a larger portion of the laser pulse energy is used to heat up the plasma. When comparing the minimum incident energy obtained through resonant multiphoton ionization of H_2 and O_2, it is reported that oxygen is ionized with approximately 0.3 mJ while hydrogen with approximately 0.6 mJ.

2.2.4 Laser-induced spark ignition

Laser spark ignition is probably the most useful method for practical applications due to not being necessary the tuning of the laser's wavelength. The process begins with multiphoton ionization of a few gas molecules which release electrons that readily absorb the laser's energy via the inverse bremsstrahlung process, increasing their kinetic energy. These accelerated electrons collide with other molecules and atoms ionizing them, releasing more electrons, which then accelerate and repeat the process. This creates an electron cascade leading to a plasma formation which then starts chain-branching reactions and igniting the mixture.

Multiphoton ionization processes are in some cases essential for the initial stage of breakdown because photon energy is in the Infrared band, while the ionization energy is in the ultraviolet band. The presence of impurities, as aerosol, dust or soot, for example, can significantly facilitate the generation of these initial electrons. When using ultrashort pulses (picosecond order) the multiphoton process must provide electrical breakdown all by itself, since there is insufficient time for electron-molecule collisions to occur and forming the electron cascade process, while with nanosecond pulses there is time for electron-molecule collision to generate more electrons, through the electron cascade mechanism. Loss processes such as electron diffusion, radiation, collisional quenching of excited states, among others, are present and can increase the effective ignition energy. A spark originated by this means is a source of highly reactive chemical intermediates at very high pressure and temperature. This spark emits light, heat and shock wave to the surrounding medium, resulting in an ignition kernel. A sufficiently strong kernel permits a transition into full scale combustion. Lee et al. in [19] used glass fibers coated with different materials to study the plasma composition influence on minimum ignition energy. They conclude that minimum ignition energy was independent of the constitution for short pulses, while for longer (1 ms) the presence of inhibitors could extinguish the flame.

Syage et al. in [20] studied ignition of hydrogen-air and hydrogen-air-CO_2 mixtures using different pulses. The results show pulses duration below 15 ns and laser's wavelength do not affect the process and the minimum ignition energy. Spiglanin, MCilroy et al. [21] investigate the shape and the structure of developing flame kernels as function of time and mixture composition in laser-induced spark ignition in hydrogen-air. As stated by the authors, gas motion dominates early flame kernel growth but, the ignition's success depends on the chemistry of the reactions, which determines if the gas transits from hot plasma to propagating flame or not. Phuoc and White in [22] studied the ignition probability dependence on the ignition location for a diffusion jet flame. A important conclusion they state is that as long as the pulse energy is enough to create 100% gas breakdown probability higher energy does not affect the observed distribution of the ignition probability. Thus, the distribution of ignition probability is mostly likely attributed to local variations of air:fuel equivalence ratio within the jet. Turbulence intensity and velocity gradient at the ignition location also influence ignition probability.

Minimum laser intensity

For an electric breakdown to occur in a gaseous mixture initial electrons are required in order to start an electron cascade. As stated before, these electrons may come from a process called multiphoton ionization, where a molecule absorbs laser photons and become ionized. A significant wavelength dependence is expected as this is a quantum effect. Srivastava in [2] state that for the first electron to be produce by multiphoton ionization the irradiance, I, should be of the order 10^{14}W/cm^2. This high value is expected because the ionization energy is much larger than the energy of a single photon. Ionization energy of O_2 molecules is 12.07 eV, of whereas a typical Nd:YAG laser with λ_0=1064 nm has a photon energy of 1.16 eV. Thus, 10 ou more photons are need to produce one free electron.

Experiments and studies done by many different authors report different values for breakdown intensity, yet always orders of magnitude below 10^{14}W/cm^2. For example, Srivastava reports the intensity

in the focus to be of 10^{12}W/cm^2, while Phuoc in [23] even stats 10^{11}W/cm^2 to be sufficient. Several authors, [24, 25, 26, 27, 2], defend that this seed electron do not come from multiphoton ionization but from impurities in gas mixture (e.g. dust, aerosol or soot particles). This hypothesis is supported by a non-dependence of the minimum pulse energy (MPE) with the laser's wavelength, and, a strong pressure dependence reported in [26, 22, 27, 28, 29], where multiphoton ionization predicts a very weak dependence. Ronney in [5] estimated the minimum ignition energy for developing a flame kernel, which is proportional to the gas density, meaning proportional to the gas pressure. On the other hand its thermal conductivity and specific heat reduce this increase, leading to a very weak pressure dependence. The experimental data disagrees and Kopecek et al.in [27] report a dependence of the form $I \sim p^{-1/m}$, $m \approx 1$.

Seed electrons

Seed electrons may origin from different laser-particle interactions. As discussed before some seed electrons come from chemical thermodynamic equilibrium, others are originated from multiphoton ionization of molecules or impurities. When the laser passes through the mixture it ionizes the impurities leading to electron emission, as referenced above. The existence of seed electron is a key factor in explaining the phenomena behind laser-induced spark ignition. If they do exist, the electron cascade occurs with much smaller laser intensities than the ones required to ionize a gas directly without a tuning of the laser's wavelength.

2.3 Gas breakdown

We have already stated that a powerful laser whose irradiance is of $> 10^{11}$ W/cm^2 interacts with a gas, and can ionized it. Whenever ionization occurs a light flash and sharp acoustic sound are observed, similar to that of an electric spark discharge. Although, laser-induced spark are smaller, shorter in duration and produce larger temperature and density gradients.

As already stated, this spark is created by the multiphoton ionization process, (MPI) and/or electron cascade process. Let's consider the electron density, n_e, its time variation is governed by:

$$\frac{dn_e}{dt} = W_{\text{MPI}} N + n_e(\nu_i - \nu_d - \nu_r n_e) \quad , \tag{2.11}$$

where W_{MPI} is the multiphoton ionization rate per atom, N the neutral atom density, ν_i the total ionization frequency due to single-impact collisions between electrons and atoms and due to electron impact excitation to the first excited state followed by photoionization, $\nu_r n_e$ is the recombination rate, where the plasma approximation is used so $n_e \approx n_i$, finally, ν_d is the diffusion rate. All this rates are function of pressure. For a weak field, the rate at which the electrons gain energy is insufficient so they can ionize the gas before diffuse out of the spark region. Therefore, a strong enough field is required to ionize the gas and to avoid the loss mechanism, yet, a field confined in a small volume increases diffusion losses. Diffusion losses are most important at low pressures where electrons diffuse rapidly,

since there are fewer gas molecules to ”hit” along its way. Energy losses can also occur from vibrational or rotational excitation of molecules.

Multiphoton ionization (MPI) process is when a gas molecule/atom absorbs several photons in a very short time interval. If the absorbed energy is larger than the ionization potential, then, the molecule is ionized and a free electron is created. MPI has been studied by several authors, such as the ones in [30, 31, 32], and we will not further develop this theory other than present it. The majority of authors calculate W_{MPI} using m-order perturbation theory, and the transition probability for m photons to be absorbed as

$$W_{\text{MPI}} = AF^m \quad . \tag{2.12}$$

For the ionization to occur the absorbed energy must surpass the ionization potential, $m > \varepsilon_i/h\nu + 1$. Bebb and Gold in [33] conclude that MPI may provide the first electrons, but, this does not account for the complete breakdown process, with exception for very short wavelength (< 1 μm) or low pressure ($<$ 1 kPa), where collisional effect are negligible.

Morgan in [30] considered an unit volume illuminated by a spatially uniform, temporally constant laser beam whose photons have energy equal to $h\nu$ with a flux F photons/cm^2-s, then solved a series of coupled rate equations for N atoms. These equations were solved assuming that an atom in a particular time could absorb enough photons to be ionized, another may absorb photons and be in a higher-energy virtual state, while others absorb up to none at all. This higher-energy states can decay, via spontaneous emission, to a lower energy at a rate ζ_r , whose mean lifetime $\tau_{l,r}$ is given by the uncertainty principle $\zeta_r \approx r/\tau_{l,r}$, with r the atom state, it can also decay via stimulated emission. Assuming a photon absorption cross-section for an atom to transit from state r to $r+1$ to be σ_r, the following equation holds for r=0 to $m-1$, where at $r = m$ we get the stable ionized state:

$$W_{\text{MPI}} = \frac{\sigma^m F^m \tau_l^{m-1}}{(m-1)!} = AF^m \text{ , where } A = \frac{\sigma^m \tau_l^{m-1}}{(m-1)!} \ . \tag{2.13}$$

The ionization rate can be enhanced through many effects. Strong electromagnetic fields results in Stark shifting and broadening, which increases the spectral line width, another effect is the overlapping and merging of the upper energy levels into a quasi-continuum spectrum. Additional effects can be produced from the laser modes of operation. In a Q-switch laser the pulse is composed by several cavity modes, and the larger the number of modes the larger the coherence of the beam. Picosecond pulses are composed of larger cavity modes than nanosecond pulses, improving the beam's coherence. A more coherent beam has local fields which exceed the average value over the focusing volume, and this leads to constructive interference over the pulse. All this is supported by the fact that femtosecond laser pulses have significantly higher ionization efficiency than nanosecond pulses.

2.3.1 Electron Cascade process

We already discussed the electron cascade process, where seed electrons, generated by either MPI or ionization of impurities, soot, aerosol particles, organic vapours, dust, p. e., gain energy via inverse bremsstrahlung (IB) and ionize more molecules. The gas electrical breakdown occurs when a significantly fraction of the gas, 10^{-3}, is ionized, or when we have an electron density of 10^{16} electrons/cm^3. The cascade ionization process is more significantly at higher pressure and for longer laser pulses, since electron-atom or electron-ion collisions have a characteristic time of the microsecond order. To Morgan in [30] the condition for gas breakdown is the product of gas pressure p and laser time pulse duration Δt_{pulse}, $p\,\Delta t_{pulse} > 10^{-7}$ torr·s.

The electron density time evolution can be analyzed through two different approaches, continuous/classic absorption process and the quantum mechanical process. The first is valid when the energy of a single photon is much less than the average electron energy, the other is valid otherwise. The average electron energy is considered to be one fourth of the ionization energy ($1/4E_{ionization}$). We will only analyze the latter, since photon energy for a Nd:YAG laser at 1064 nm is 1.16 eV and the average electron energy for a hydrogen atom is 3.4 eV, thus, the classic approach is invalid. The quantum approach starts from the Boltzmann equation and takes into account the discrete energy of the laser beam photons as presented by the authors of [34, 35, 36, 37]. Dalgarno and Lane in [36] relate the inverse bremsstrahlung absorption coefficient, K_a (cm^5), to the momentum-transfer cross-section σ_m through

$$K_a = 6.0 \times 10^{-25} \lambda_0^2 (\varepsilon + h\nu)^{1/2} \left[\left(1 + \frac{\varepsilon}{h\nu} \sigma_m(\varepsilon) + \frac{\varepsilon}{h\nu} \sigma_m(\varepsilon + h\nu) \right) \right] \tag{2.14}$$

where ε is the electron energy in eV, $h\nu$ the photon energy in eV, σ_m the momentum transfer cross-section in cm^2, and λ_0 the laser wavelength in μm. Photons can also be emitted when an electron collides with a neutral so the stimulated emission coefficient K_e is obtained from balance equation and is

$$\begin{aligned} K_e = K_a \left(1 - \frac{h\nu}{\varepsilon} \right) \left[1 - \frac{h\nu}{\varepsilon} \right]^{1/2} \quad & \varepsilon > h\nu, \\ K_e = 0 \quad & \varepsilon < h\nu, \end{aligned} \tag{2.15}$$

Rose and Weyl in [38] study and conclude that for a laser flux higher than 10^{10} W/cm^2 momentum transfer collisions are always small compared to inelastic collisions. Stimulated emission losses are only a small fraction (<10%) of the energy gained from the laser field. If all the laser's energy results in electron impact ionization, the ionization rate would be

$$\nu_i = \frac{K_a N}{\varepsilon_i} I \quad , \; I = \frac{c\vec{E}^2}{4\pi} \tag{2.16}$$

where I is lasers irradiance which relates to the electric field $\vec{E}$ of the laser through Poynting's theorem. K_a is computed using the mean electron energy $\bar{\varepsilon}$, and N is the gas density. Energy loss mechanisms originate in elastic and inelastic collisions, diffusion loss and recombination loss. In an

elastic collision the initial and final states are the same with only a change in its kinetic energy. Elastic loss $(L_e)_{elastic}$ is given by the following equation from [39],

$$(L_e)_{elastic} = \frac{2m_e}{M}\overline{\varepsilon}\nu_m \quad , \tag{2.17}$$

where M is atom's mass, m_e the electron mass, ν_m the electron momentum transfer collision frequency and $\overline{\varepsilon}$ is the average electron energy.

When an inelastic collision occurs, the internal state of the atom is changed after the kinetic energy exchange. If an atom stays in the excited state long enough and does not leave the focal volume, it may be photoionized or ionized by a further inelastic collision. The atom can radiate as its energy is reabsorbed by neighbouring atoms. Chan et al. in [39] argued that an excited atom can lost its energy through two different ways, the first independent of the focal volume and the second depends on the focal volume and diffusion length Λ. Combining these, the following equation arises

$$(L_e)_{inelastic} = \frac{\varepsilon_i}{\ln 2}\left(\alpha + \frac{\beta}{\Lambda^2}\right)\nu_m \quad . \tag{2.18}$$

In a previous equation, Λ=r_f/2.405 and relates to the focal radius r_f, α is a dimensionless parameter and β has dimensions of squared length. Data for α and β can be found in [39] and both parameters are one order of magnitude greater for molecular gases than for inert gases.

The electrons can diffuse out of focal volume, and this is specially important for a small focal volume and long laser flash. Diffusion loss frequency ν_d can be equated using

$$\nu_d \approx \frac{D}{\Lambda^2} \quad , \tag{2.19}$$

where D is the electron diffusion coefficient (cm^2/s). Electrons diffuse more freely at lower density, and from kinetic theory of gases is possible to estimate D as

$$D = \frac{1}{3}\frac{\overline{v}^2}{\nu_m} = \frac{2\overline{\varepsilon}}{3m_e}\frac{1}{\nu_m} \quad . \tag{2.20}$$

The momentum transfer frequency ν_m can be estimated using gas kinetic cross-section σ_s as

$$\nu_m \approx N\sqrt{\frac{2\overline{\varepsilon}}{m_e}}\sigma_s \quad , \tag{2.21}$$

where N can be estimated by $N = N_0 p$, proportional to the pressure p. By recalling Eqs.(2.19) and (2.20) we obtained that D is proportional to p^{-1} and Λ^{-2}, so when equating n_e diffusion losses are minimized at higher pressures. This statement agrees with what we have already presented that higher filling pressures are easier to ignite.

As electrons diffuse out of the focal volume, the remaining ions create a space charge effect. For a large enough space charge electrons cannot diffuse freely, and have to drag the ions along. Diffusions became ambipolar, and D is reduced by $\sqrt{m_e/M}$. The ion space charge is only important at higher electronic density, where ion density is also greater.

The final loss mechanism we will present is the attachment loss. Many molecular gases can attach electrons to become electro negative. This mechanism occurs through three-body attachment or two-body dissociative attachment. Electron-ion recombination is important in the latter stages of electron cascade, when both electron and ion densities increase, determining the development of the cascade itself. The attachment rate can be calculated through

$$\nu_r = 8.8 \times 10^{-27} \frac{n_e^2}{T_e^{3.5}} \quad , \tag{2.22}$$

with T_e the electron temperature in eV, n_e the electron density in cm^{-3}.

2.3.2 Threshold Calculation

To understand laser ignition from both a fundamental point of view and application/engineering, it is important to determine the conditions for which a spark is produced. The knowledge is crucial to design and select laser, optics and beam delivery systems for practical applications. Starting with Eq. (2.11), considering MPI as the only electron source and $N = N_0 p$, we get

$$\frac{dn_e}{dt} = W_{\text{MPI}} N = \frac{\sigma^m F^m \tau_l^{m-1} N_0 p}{(m-1)!} \quad . \tag{2.23}$$

Considering a constant photon flux of duration τ_p, and solving Eq. (2.23) in order to the flux F gives,

$$F = \frac{1}{\sigma \tau_l} \left[\frac{n_e \tau_l (m-1)!}{N_0 p \tau_p} \right]^{1/m} \quad . \tag{2.24}$$

Is simple to conclude that MPI breakdown threshold depends on gas pressure as $p^{-1/m}$. For a Nd:YAG laser at 1064 nm, the energy of a single photon is 1.16 eV, so most gases required 14 photons to be ionized. Therefore MPI has a pressure dependence of $p^{-1/14}$, very weak. Grey-Morgan in [30], reported that the critical number of electrons for gas breakdown is about 10^{16} electrons/cm^3 or a fraction of $n_{e,cr}/N_0 p = 10^{-3}$. Comparing it with experimental data for $\sigma = 10^{-16}$ cm^2, $\tau_l = 10^{-15}$s, $\tau_p = 10^{-9}$s and a fraction of 10^{-3}, that implies a threshold flux $F_{th} > 10^{30}$ photons/cm^2·s, which is generally within an order of magnitude of the experimental data.

2.3.3 Energy transfer to plasma

Bradley et al. in [40] observed the time evolution of a potentially igniting kernel through an Imacon schlieren photography of a non igniting propane-air mixture λ=2.22, at 300 K and 0.1 MPa of filling pressure. The author used a laser pulse with a duration of 15 ns, yet, most of the energy transfer occurred in about 10 ns. The schlieren imaging revealed an electric breakdown followed by a very rapid heating of the plasma and a shock wave generation. Similar to traditional spark ignition, initially there is a rapid creation of a high temperature plasma. The plasma first contracts due to its high rate of radiative loss. Eventually, the kernel starts to expand radially by conduction. The formed plasma kernel has cylindrical shape with length l and height h orthogonal to it. In the first stages $l > h$, Bradley et

al.'s studies and photographs, reproduced in Fig. 2.2, show that as time $t \to 0$, $h/2 \to r_0$, with r_0 the initial shock wave radius. As time passes, the plasma kernel contracts in the longitudinal direction l and expands in h, until it acquires a more rectangular shape.

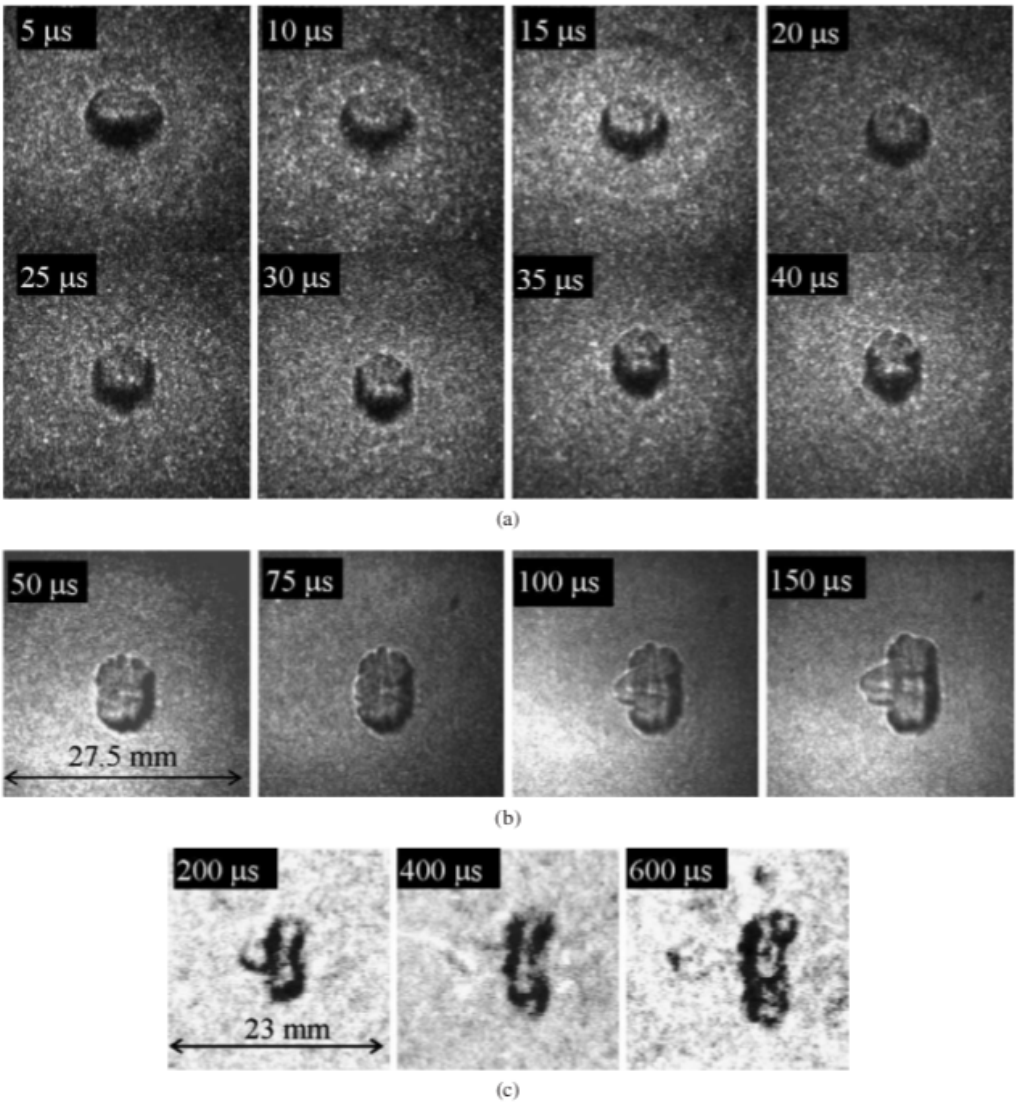

Figure 2.2: Photographic images of kernels.

(a, b) Imacon schlieren images of nonigniting propane–air mixture, λ=2.22 (c) Hitachi schlieren images in air. Time measured from laser pulse, incident laser energy 224 mJ, in [40].

It is expected that the size of the initial plasma kernel to be related to electric breakdown mechanism and the transferred energy. The longitudinal dimension l should be related to the absorption length of the plasma, the inverse of the absorption coefficient $k'_{e,i}$, for which the laser energy flux decays to 1/e of its original value. Once the electrical breakdown occurs the plasma is highly opaque to the laser's light and easily absorbs it, as stated before, the process for this absorption is the inverse bremsstrahlung, for temperatures inferiors to 10000 K the electron density is low and electron-neutral inverse bremsstrahlung dominates. In this regime the effective absorption coefficient $k'_{e,n}$ is taken from [41] and given by:

$$k'_{e,n} = \left[1 - \exp\left(-\frac{hc}{\lambda_0 k_B T}\right)\right] \sum_j \sigma_j n_e n_j \text{ cm}^{-1} \quad , \tag{2.25}$$

where n_e and n_j are the electron and jth neutral atomic species densities (cm^{-3}), respectively, σ_j is the average cross section for absorption of a photon of wavelength λ_0 (cm) by an electron during a collision with species j (cm^5), k_B is the Boltzmann's constant (1.38 $\times 10^{-16}$ erg-K^{-1}), h is the Planck's constant (6.625 $\times 10^{-27}$ erg-s), c is the speed of light (2.998 $\times 10^{10}$ cm s^{-1}) and T is the temperature (K).

Whenever the temperature rises above 10000 K, electron-ion inverse bremsstrahlung becomes dominant and its absorption coefficient $k'_{e,i}$ is given by:

$$k'_{e,i} = \left[1 - \exp\left(-\frac{hc}{\lambda_0 k_B T}\right)\right] \frac{4e^6 \lambda_0^3}{3hc^4 m_e} \left(\frac{2\pi}{3 m_e k_B T}\right)^{1/2} n_e \sum_i z_i^2 n_i g_i \text{ cm}^{-1} \quad . \tag{2.26}$$

In this equation z_i and n_i are the charge and density of the ith ionic species, m_e the electron mass (9.109 $\times 10^{-28}$ g), e, the electron charge (4.803 $\times 10^{-10}$ esu) and g_i the Gaunt factor, a corrective factor usually of the order of unit. Using the relation, $\sum_i z_i^2 n_i g_i = n_e$, the previous equation can be simplified, and considering a Nd:YAG laser at 1064 nm, it becomes

$$k'_{e,i} = 0.1645 \times 10^{-34} \frac{n_e^2}{T^{1/2}} \left[1 - \exp\left(-\frac{13500}{T}\right)\right] \text{ cm}^{-1} \quad . \tag{2.27}$$

With the increase of the electron density, the respective plasma frequency increases as well. If the plasma frequency is equal to the laser frequency, light will be reflected and will not heat the kernel. The plasma frequency ω_p is calculated through,

$$\omega_p = \left(\frac{4\pi n_e e^2}{m_e}\right)^{1/2} = 56413\sqrt{n_e} \quad \text{s}^{-1} \quad . \tag{2.28}$$

From this, it is trivial to solve it in order to n_e and compute the critical electron density n_c for which the two frequencies are equal and the laser is reflected. We will consider a typical Nd:YAG laser, since it is the most common used in laser ignition and the one that was used in the ESTHER project,

$$n_c = 2.495 \times 10^{19} \text{ cm}^{-3} \quad . \tag{2.29}$$

In order to evaluate $k'_{e,i}$ we need to have prior knowledge of both T and n_e. These can be obtained from the electron energy equation, but is a complex treatment so many authors assume $n_e = n_c/4$, namely Ma in [42] assumed this and T_e=600000 K. The mathematical procedure is to estimate values of T and n_e after the energy cease at 15 ns from the experimental data using blast wave theory. So, the inverse bremsstrahlung absorption coefficient can be computed in reciprocal order, and then, compared with the measured plasma lengths from several conditions.

2.3.4 Shock-wave generation and propagation

A laser pulse deposits its energy in about 10 ns, for an energy input of 0.2 J a sphere of radius 2.7 mm has an average power of 240 TW m^{-3}, five orders of magnitude higher than the average spark-plug and much higher than the volumetric heat released rates in combustion. During the time interval between electric breakdown and the end of the laser pulse, the plasma and shock wave fronts propagate with $t^{2/5}$. The shock wave growth is controlled by the laser's energy input.

The shock-wave propagation can be modelled with the classical blast wave theory of Taylor, as in [43]. The author assumes an instantaneous energy transference to a point-like volume. The validity of this model is greater after the pulse duration but, as it propagates, the pressure ratio decreases and this self-similar expressions become invalid. Nonetheless, this theory presents relations between shock wave radius r_s and time t, from the initial time instant when the energy E is deposited,

$$r_s = s(\gamma) t^{2/5} \left(\frac{E}{\rho_0} \right) \quad , \tag{2.30}$$

where $s(\gamma)$ is a constant of order 1, function of heat capacity ratio, and ρ_0 is the gas density ahead of the shock wave. Performing the time derivative of Eq. (2.30) to obtain the shock wave velocity v_s, we get:

$$v_s = s(\gamma) \frac{2}{5} t^{-3/5} \left(\frac{E}{\rho_0} \right)^{1/5} \quad . \tag{2.31}$$

When comparing blast theory with the experiments and imaging of the schlieren photographs, Bradley et al., in [40], conclude that a fit to Eq. (2.30) was compatible with experimental data. The best fit reported yield a time exponent of 0.38 and E=0.154 J, which implies that 85% of the energy absorbed by the plasma is used in the shock wave. The deposited energy was measured by the difference between pulse energy and transmitted energy, and they obtained 0.18 J. The shock wave maximum temperature T_s and pressure p_s can be calculated using Rankine-Hugoniot relations:

$$\begin{aligned} \frac{p_s}{p_0} &= \left(\frac{2\gamma}{\gamma+1} \right) \left(\frac{v_s}{c_s} \right)^2 - \left(\frac{\gamma-1}{\gamma+1} \right) \quad , \\ \frac{T_s}{T_0} &= \left[\left(1 - \left(\frac{c_s}{v_s} \right)^2 \right) \left(\frac{\gamma-1}{\gamma+1} \right) + 1 \right] \times \left[\left(\left(\frac{v_s}{c_s} \right)^2 - 1 \right) \left(\frac{\gamma-1}{\gamma+1} \right) + 1 \right] \quad , \end{aligned} \tag{2.32}$$

where c_s is the acoustic speed $= \sqrt{\gamma R T_0}$, with R the ideal gas constant divided by the molar mass. It is possible to compute v_s recurring to Eq. (2.31), and then the values for p_s and T_s. Bradley et al. reports that as $t \to 0$ the plasma becomes fully ionized, and the electron density is calculated through the equation of state. Through Eq. (2.27) is possible to calculate the value of $k'_{e,i}$ and estimate the absorption length, $k'^{-1}_{e,i}$. The values for the absorption length and the measured l_0 do not agree. Bradley et al. suggests that the effective absorption length is created at $t < 15$ ns, while the electron temperature is higher, meaning longer absorption lengths.

2.4 Applications of laser ignition

In the last Section a mathematical model was presented to describe the spark formation and development relating it to the mixture and laser properties. Clearly, many difficulties arise from solving the Boltzmann Kinetic equation and even semi-empirical models do not fully comprehend the Physics. In most practical applications a full theoretical model is not needed, nonetheless, a more complete and agreeable model with experimental data should be developed to understand how and where the laser energy is deposited.

2.4.1 Laser-induced plasma evolution

After the electrical breakdown the plasma kernel expands due to the absorption of the laser energy. The kernel in practice is not spherical, but as reported by Bradley et al. in [40], it is an elongated ellipsoid with the major axis along the laser beam. In truth, the spark tends to acquired a cone-like shape, whose base is behind the focal point, towards the lens as observed by Phuoc and White in [22]. This cone-like shape is more pronounced and larger as the pressure increases, as depicted in Fig. 2.3. This indicates that inverse bremsstrahlung is dominant, leading to the kernel expansion itself. As the spark is rapidly heated, the thin layer of outermost plasma raises to very high temperature and pressure, expanding the layer. For a sufficiently fast heating a shock wave is generated, which moves supersonically into the cold gas. As it propagates, the shock heats and weakly ionizes the gas, then becoming opaque to the laser. The ionized gas absorbs the energy immediately before the shock front.

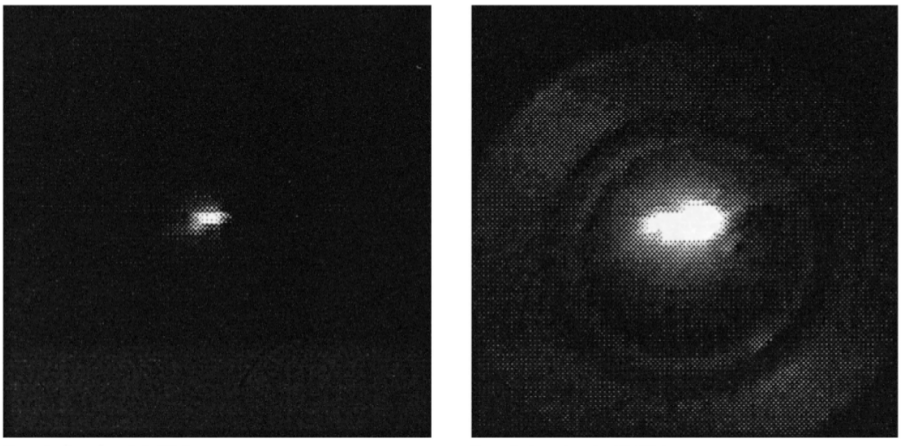

Figure 2.3: Spark size as function of pressure, in [28]

Another characteristic of the spark is its size as function of air:fuel equivalence ratio, Phuoc and White in [22] studied ignition in methane-air mixtures at 1 atm. The results, depicted in Fig. 2.4 show that the spark is smaller near the stoichiometric conditions, increasing towards both rich and lean mixtures. On the methane-lean and rich sides, the spark had an oval shape, whose major axis varied from 0.8 mm to 2 mm, and minor axis from 0.4 mm to 1.2 mm, function of the methane fraction. For a stoichiometric or near-stoichiometric methane-air mixture, the spark becomes cylindrical with 0.3 mm of radius and 0.8

mm of length. The authors also measured that for a laser shot of 270 ns to 350 ns, the spark's life time was about 5 to 11 μs, depending on the laser's energy. The spark tends to separate into several points along the beam, often behind the focal point.

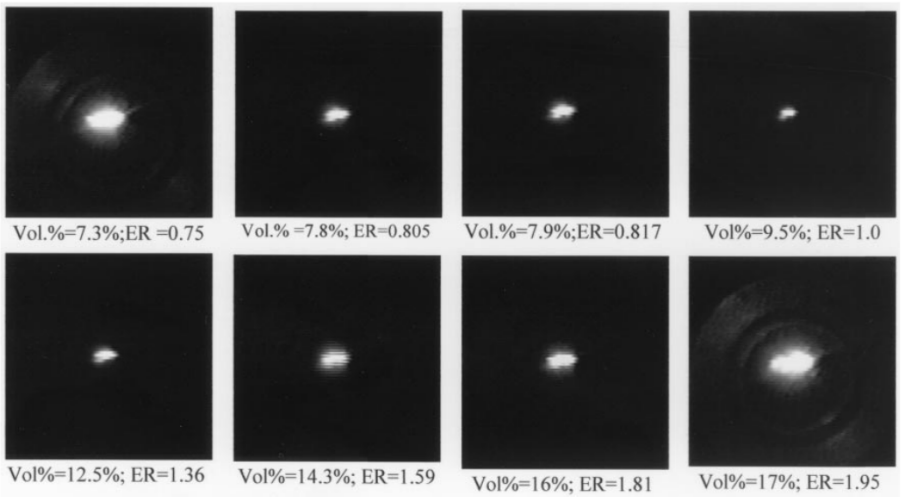

Figure 2.4: Spark size as function of λ, in [22]

2.4.2 Laser characteristics for a practical application

For a reciprocal engine the concept of a laser ignition system was originated in the late 60's. The possible practical systems have been conceptualized and studied by Tauer in [25], between several approaches, two of them are:

- An individual ignition laser is mounted on each cylinder head supplied by and external pump source;
- Laser unit is external to the engine, and the pulses are transported via optical fiber to the cylinders.

In both cases the laser system must be compact and robust to sustain the engine vibrations and adverse cylinder head influences. Other than that, to be viable a laser ignition system must not be more complex or expensive to maintain than a typical spark plug. A typical diode pumped laser can work up to 10000 h. In comparison, a spark plug in average has 1000 working hours, as Weinrotter et al. presents in [24].

In chapter 2.2 several laser ignition mechanisms were presented. For practical applications electrical breakdown is the chosen method mostly because it does not required a fine tuning between the laser and the gases mixture absorption wavelengths. As established before, the main requirement of a laser ignition system to perform electric breakdown and then ignition is the irradiance. Different values for this are presented by several authors, it is important to notice that the initial conditions differ and that is a key factor. Phuoc in [23, 28, 22] reports that electrical breakdown can be achieved with 10^{11} W/cm^2, while Weinrotter et al. in [24] reports breakdown at 10^{14} W/cm^2. Kopecek et al. in [26] reports the non dependence of minimum pulse energy (MPE) and efficiency on the laser wavelength. This is also supported in [24, 27, 25, 42]. Thus, the choice of laser medium and wavelength is mostly due to its

focus and pulse time width rather than the wavelength itself. The generation of short pulses in the order of the ns is well achieved by passively Q-switched lasers. Ma in [42] used three different lasers and calculated the different irradiances. The author used a Nd:YAG (1064 nm), an excimer ArF (193 nm) and a KrF (248 nm), for the same pulse energy the peak power and peak intensity were compared. The Nd:YAG laser had a FWHM of 7 ns when comparing with the 17 ns of the excimer lasers, therefore, a peak power of 13 and 5.4 ($\times 10^6$) W, respectively. Besides this, a Nd:YAG has a beam divergence angle of 0.5 mrad while the excimer has a beam divergence of 2 mrad. In pratice this makes a focal spot diameter of Nd:YAG three times smaller than the one of the excimer. A smaller focal spot size implies a higher irradiance, which means that good quality beams can be used with less energy and still ignite the mixture. Naturally a solid state laser arises in comparison to an excimer laser for both mechanical resistance and pulse width, and since there is no wavelength dependence Nd:YAG is a possible solution due to being high power and commonly used.

To achieve full scale combustion high powers are needed. This represents a problem with pulse transportation, first the typical mirror and the lens optical systems are no flexible and very sensitive to vibrations and misalignment, thus, not feasible to a real solution. Optical fibers ensure as a natural solution to this problem but, as a matter of fact, the damage threshold of the fiber material is a limitation to this solution. The typical breakdown threshold for fused silica fiber is about 1.5×10^9 W/cm^2, at least one order of magnitude behind the minimum breakdown report. Larger fiber optics can be used so higher powers can be transported, but this implies multi-mode beam profiles, which are disadvantageous in the focusability of pulse and possible formation of hot spots along the fiber, as referred in [23]. A possible solution is to have the laser gain medium incorporated in the cylinder head, and the pump source connected via optical fibers to it. Since the pump has much lower power, it can be safely transported from the source to the gain medium and only near the combustion chamber the laser pulse is produced and focused. Unfortunately, small lasers with laser pulses are not commercially available. These are large, heavy, expensive and consume kilowatts of electric power. Tauer in [25] presents a design and image for a potential laser-plug in a cylinder bank, which we reproduce in Fig. 2.5. Lastly, the window between the laser oscillator and the combustion chamber needs to be transparent to the appropriated wavelength. A important issue is that combustion soot and other particles start to accumulate on the window and lead to substantial absorption of laser radiation, which translates in a efficiency loss.

2.4.3 Combustion properties for laser-induced ignition

We have already defined air:fuel equivalence ratio, λ, and for a combustible mixture at specific conditions the minimum and maximum values for which λ ignites are define the rich and lean flammability limits, respectively. In theory, these limits do not depend on the ignition source, but in practice that is not true. When designing a laser ignition system the minimum pulse energy (MPE) is one of the most important specifications to account for. Given a specific set of optical elements and mixture parameters (gases, λ, temperature, filling pressure, ...) MPE is the pulse's energy for which a given or higher ignition probability is achieved (usually 50%). This is a relevant area of study because using a less powerful

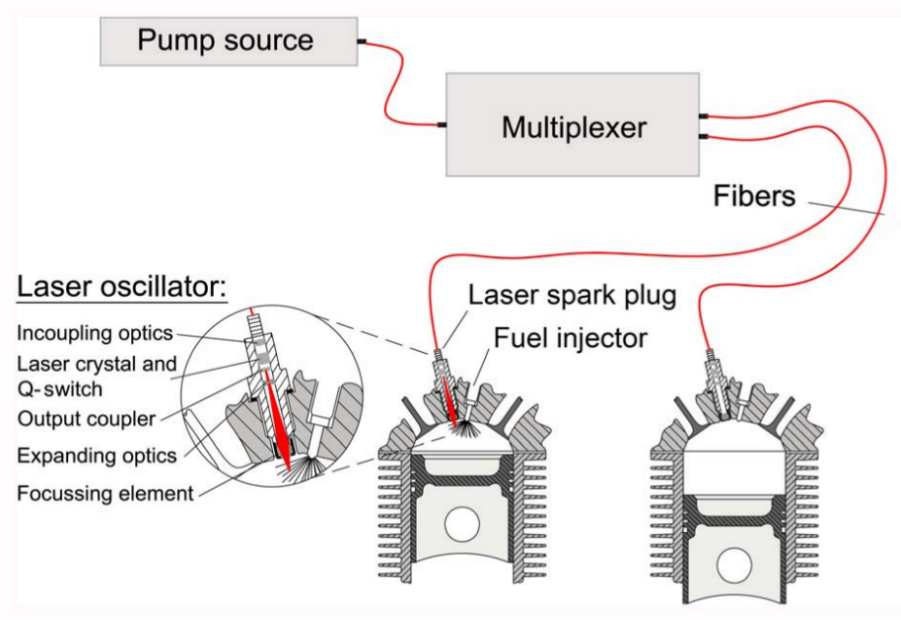

Figure 2.5: Schematic design for the conceptualize laser ignition system in a reciprocal engine. An external pump source supplies an individual laser in each cylinder head, controlled by a multiplexer, in [25].

laser is advantageous, as it is simpler, smaller, lighter. It is important to differentiate minimum pulse energy (MPE) from minimum ignition energy (MIE) which is the effective energy used in ignition, if the optical system was 100% efficient, no power losses, and all the laser's energy were deposited MIE would be equal to MPE.

When using hydrogen as fuel, it is of high interest to study lean high-pressure combustions, as they produce less pollutants and are more efficient. Other than that, safety is crucial in every application and hydrogen ignites easier than most hydrocarbons, especially in rich or stoichiometric environments. Weinrotter et al. in [24] performed experiments in a closed chamber at 1 MPa of filling pressure, varying λ between 1.8 and 8. They state that ignition could be achieved for at least λ=8, Dharamshi in [44] also recorded ignition for λ=5. Bradley et al. in [40] studied the influence of pressure on the lean flammability limit for isooctane-air mixtures, his results show that increasing pressure increases the flammability. Hydrogen behaves in a similar manner as Xueling reports in [45].

Knocking is the phenomena where combustion does not only propagate as a spherical flame front originating from the plasma but also explodes, generating shock waves, at different locations in the unburned gas as an effect of self-ignition conditions. These self-ignition conditions are easily observed as a rapid oscillation in the pressure, whose frequency is the resonant frequency of the combustion chamber itself. The authors of [24] recorded this behavior for λ between 2.5 and 3.6 at 1 MPa of filling pressure, and explained that it is due to the higher flame velocities of richer hydrogen mixtures. Because of the higher velocities, as it propagates the flame produces high-pressure and temperature regions in the unburned gas, leading to self-ignition. In engine applications knocking is extremely disadvantageous, causing power loss and damaging the engine. The authors of [24] study, as well, the influence of the filling pressure in knocking, fixing λ=3.5, knocking was not observed for filling pressures equal or

higher than 1.8 MPa. Nonetheless, knocking occur when using a richer mixture (λ=3), in spite of filling pressures of up to 2.8 MPa. Srivastava, in [2], also register knocking in similar conditions to Weinrotter et al., with 3 MPa of filling pressure and λ=3.

Two-stage ignition is a possible occurrence in laser ignition. This phenomena was observed and identified by Weinrotter et al. in [24]. For a determined initial conditions when the gas, as it burns, achieves a specific pressure value a high quantity of H_2O_2 molecules are produced. These molecules are non-reactive in a pressure window, and so, slows down the combustion rate. If another specific pressure value is then reached, the molecules of H_2O_2 dissociate into highly reactive OH radicals, rising the combustion speed again. This phenomena is detected by observing the pressure rising velocity in the combustion chamber over time. Both knocking and two-stage combustion can be identified in Fig. 2.6. The influence of different initial parameters in the characteristics of a closed vessel combustion is summarized in Tab. 2.1, taken from [24].

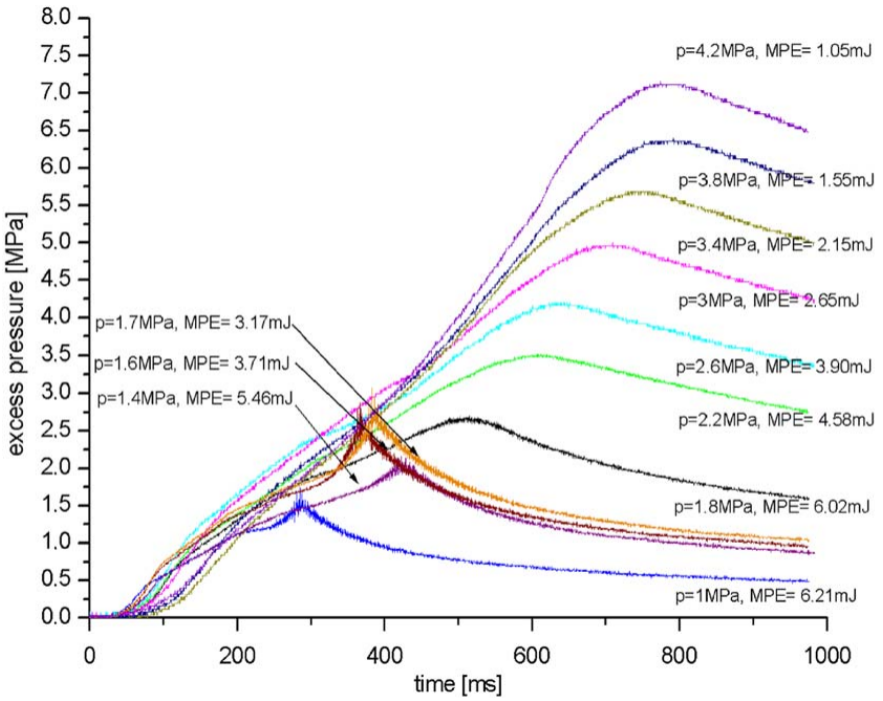

Figure 2.6: Pressure signal over time at MPE for λ=3.5, initial temperature 473 K, and varying pressure between 1 and 4.2 MPa.

Knocking is observable for pressures smaller 1.8 MPa and two-stage combustion in p=1 MPa, in [24].

We already stated that speaking in terms of minimum ignition energy might not be fully accurate in practical scenarios. Studies have been carried out by investigating the various energy fractions of laser-induced spark ignition and the respective loss mechanisms. Phuoc and White in [46] studied these loss mechanisms in air sparks from 15 mJ to 60 mJ, their results are presented in Tab. 2.2.

Table 2.1: Combustion characteristics function of its initial parameters

	Peak Pressure	MPE	Time until peak pressure	Ignition delay
$\lambda \uparrow$	$\downarrow$	$\uparrow$	$\uparrow$	$\uparrow$
$p \uparrow$	$\uparrow$	$\downarrow$	$\uparrow$	$\uparrow$
$T \uparrow$	$\downarrow$	$\downarrow$	$=$	$=$
PE $\uparrow$	$=$	$=$	$=$	$=$
Focal length $\uparrow$	$\uparrow$	$\uparrow$	$\downarrow$	$\downarrow$
Plasma size $\uparrow$	$\uparrow$	$\uparrow$	$\downarrow$	$\downarrow$

$\uparrow$, increasing; $\downarrow$, decreasing; $=$, no significant change in the combustion process; λ air:fuel equivalence ratio; p, initial pressure in the combustion chamber; T initial temperature of the combustion chamber; PE, laser pulse energy; MPE, minimum pulse energy to achieve ignition; ignition delay, time until 5% of peak pressure is reached, in [24].

Table 2.2: Energy balance for a laser spark in air, in [46].

Spark energy (mJ), E_{sprk}	15	22	30	35	44	50
Shock energy (mJ), E_{shock}	10.6	15	19.2	21.8	27.1	28.6
Remaining energy (mJ), E_{ign}	1.05	1.48	2.64	2.97	3.21	4.29
E_{shock}/E_{sprk} (%)	70	68	64	62	61.6	57
Bremsstrahlung loss (mJ)	2.30	3.45	4.65	4.77	5.62	5.99
Blackbody loss (mJ)	1.04	2.06	3.49	5.44	8.05	11.1
Convective loss (mJ)	0.01	0.013	0.016	0.017	0.019	0.02
E_{loss}/E_{sprk} (%)	93	93	91	92	92.7	91.4
E_{ign}/E_{sprk} (%)	7	7	9	8	7.3	8.6

The energy fraction used effectively in ignition is less than 10%, meaning laser spark ignition is extremely inefficient. Most of energy is used to create the shock wave, and its fraction reduces as the pulse energy increases. Loss mechanisms also increase with the pulse energy, namely blackbody and convective losses.

2.4.4 Comparison of Laser vs. conventional ignition combustion properties

Clearly using laser-induced spark ignition represents a severe energy overkill, since the energy needed to ignite is at least one order of magnitude above its theoretical value. When comparing it with a spark-plug, both methods use much more energy than the theoretical minimum as presented in [40]. Due to the energies orders of magnitude this is not a major problem, nonetheless, spark-plug's power-time pulses have the potential to be controlled.

Minimum ignition and pulse energy of laser induced spark ignition are similar to those of traditional spark-plug in both far lean and far rich sides, but, consistently higher in the stoichiometric region as Phuoc and others authors present in [23, 29]. This is supported by Bradley et al. in [40], where they also state that the lean side limitations of ignition might relate to the gas dynamic. Weinrotter et al. in [24] presented the same conclusion, and argued that in the lean side the decrease in H_2 molecules leads to a decrease in the production of H radicals, making ignition less efficient. The advantage that

laser presents regarding energy is due to the MPE pressure dependence. Contrary to the spark-plug, where the voltage needed to perform electrical breakdown increases with pressure, the data in Tab. 2.1 shows that laser ignition MPE decreases with filling pressure, thus, is an advantage in high-pressure environments, supported by the studies in [5, 26, 23, 22, 27]. Besides this, erosion effects on electrodes are more significant at higher pressures, where a laser does not have that limitation.

A laser pulse deposits the energy in a nanosecond time interval, while the spark-plug deposits in a microsecond time interval. This ignition delay was observed by Ma in [42] and Kopecek et al. in [26]. Not only the ignition delay is shorter, the combustion speed increases when using laser comparing to spark-plug ignition. Typical times for each stage of combustion are presented in [24], the combustion itself can last between 1 ms to 1 second, while in contrast the pulse duration can be up to 9 orders of magnitude shorter. Srivastava in [2] compared combustion evolution for similar mixtures at 3 MPa and various air:fuel equivalence ratio using a 20 mJ laser pulse and 180 mJ 0.35 mm gap spark-plug. His results clearly show that the former achieves peak pressure in less time, meaning a faster combustion speed. The reason for this can be related to the absence of flame quenching or to the energy transferred to the gas phase. Another conclusion is combustion speed increases for richer mixtures, which is in agreement with the higher flame speed for richer mixture, both conclusion are supported by Ronney in [5]. Peak pressure were similar in both cases, decreasing for leaner mixtures as expected. Besides this, the laser-induced plasma is formed in a fixed position, while spark-plug plasma moves around the electrodes circumference. All this characteristics present great advantages for high revving engines, firstly, because shorting ignition delay and combustion time means RPM can be increase without risk of knocking, secondly because, shorter combustion time reduces heat transfers/losses through vessel walls increasing its thermal efficiency. Controlling ignition point position is also advantageous. With it ignition can start at the middle of the chamber, which maximizes the time flame is unaffected by the walls, not cooling (and reducing its thermal efficiency). It can even be possible to perform multi-point ignition.

Chapter 3

Experimental Setup

As reported in [1] ignition was achieved without a focusing lens, meaning that the laser's irradiance of 10^8 W/cm^2 is up to 4 orders of magnitude less to what the literature reports. The reasoning to this relates to the filling pressure, as ignition for low pressure could not be achieved without lens. To achieve ignition, a flame kernel must be developed with a minimum energy density, as presented in [4] and the energy must be provided by the laser. A non resonant and non focused laser cannot form a plasma through MPI process, meaning that the gas mixture must absorb energy throughout other processes. To investigate the laser absorption at high pressures, an experimental setup was designed and assembled utilizing ESTHER facilities in the Hypersonic Plasmas Laboratory. The focus of this experiment is to understand how transmittance varies for different pressures and power fluxes.

A second experiment was designed and assembled to study how minimum pulse energy and ignition probability varies as function of the air:fuel equivalence ratio for H_2-air pre-mixtures flows. This was done in the Clean Combustion Research Center at King Abdullah University of Science and Technology (KAUST), under the supervision of Professor Deanna Lacoste.

3.1 Laser absorption at high pressures in ESTHER

This first experimental setup was composed of two parts, the combustion chamber and the laser and respective optical components. The alignment was made using a diode red laser as guide, so when the red and Nd:YAG lasers are aligned the latter is turned off as a safety measure. The combustion chamber is composed of a cylindrical metal vessel with 80 mm inner diameter and 600 mm of length, with a bolted top cap having a fused silica window as laser's entry point to the chamber as depicted in Fig. 3.1. The optical setup is shown in Fig. 3.2. A cylinder was placed inside the chamber to support a 0º mirror designed to reflect the Nd:YAG laser beam. The Nd:YAG laser (Quantel Brilliant, 1064 nm, 360 mJ, 5 ns) is reflected by two 45º mirrors (High power CVI mirrors) for beam height and azimuthal deviation, passes through a half-wave plate and a beam splitter cube, then proceeds entering the chamber. It is possible to adjust the laser power sent to the chamber using the the half-wave plate and the polariser cube. The half-wave plate linearly polarizes the light and the beam splitter cube divides it as function

of the polarization, part into a beam dumper and the other in direction of the combustion vessel. Inside the chamber the beam is reflected so a measurement of its power can be performed after crossing the combustion chamber. In Appendix B we present photographs of the Experimental setup and of the experiment run.

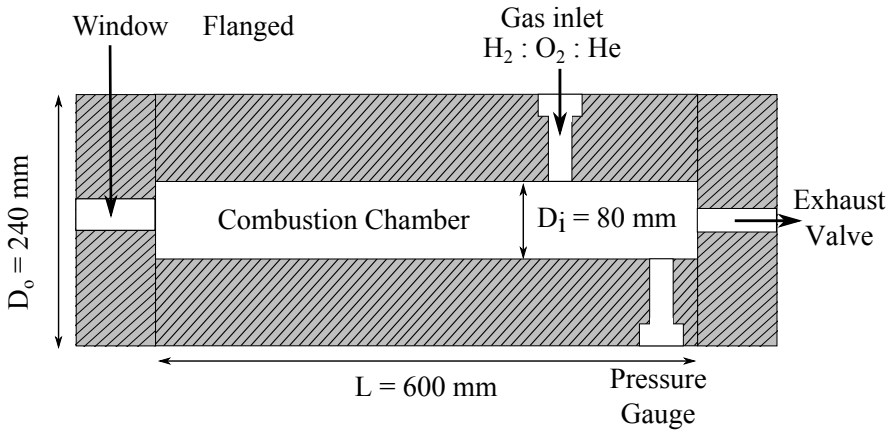

Figure 3.1: ESTHER's shock-tube test combustion chamber

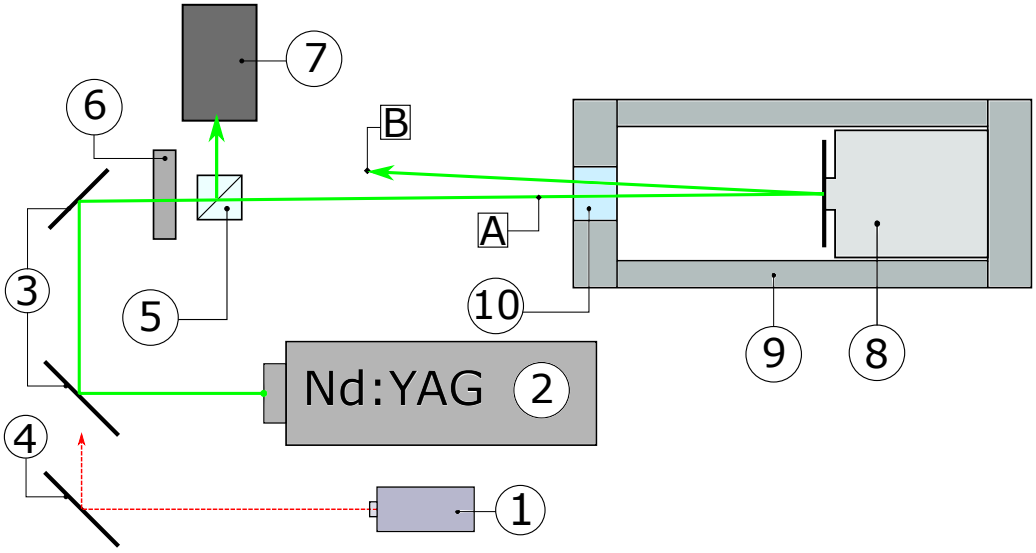

Figure 3.2: Schematic for the Laser absorption experiment.

1 - Alignment red diode laser; 2 - Nd:YAG laser (λ_0= 1064 nm); 3 - 45º mirrors; 4 - 45º mirror; 5 - Beam splitter cube; 6 - Half-wave plate; 7 - Beam dumper; 8-0º mirror and support cylinder; 9 - Combustion Chamber; 10 - Fused Silica window; A - Entry power measuring point; B - Exit power measuring point.

The experiment follows these steps:

A powermeter (Coherent Molectron Powermax 500A) was placed right before the silica window to measure the input laser power, and then placed in a point of the beam's optic path to measure the transmitted power.

Filling of the chamber with an He-O_2 [10:1] and then an He-H_2 [9:2] mixture up to a filling pressure

of 100 bar. This is done to mimic a [8:2:1] He-H2-O2 combustible mixture [1], but without the reactivity (since firing the laser in such a mixture would initiate ignition and would destroy the mirror inside the vessel). Any differences in absorption from the He-O_2 and He-H_2 experiments can be attributed to the different chemical compositions, allowing the determination of the absorptivity of the He-H_2-O_2 combustible mixture through a correlation of both partial mixtures absorptions. A round of experiments with the aforementioned He-O_2 mixture was firstly done by measuring the laser input power at point A (Fig. 3.2), followed by measuring the laser transmitted power at point B (Fig. 3.2).

The powermeter is then placed, again, at point A. The power is again adjusted using the half-wave plate and we repeat the measurements. After 5 to 10 different input powers, the pressure in the chamber is reduced using the venting valve. A second run of the experiment was then made using He-H_2 [10:1] with the same steps described above.

Finally, to evaluate any power losses through air and optical components, another run of the experiment was made with an open chamber and without the silica window, and a final run measuring the power loss between points A (P_{in}) and B (P_{out}). The values of P_{in} and P_{out} are the average power over time for a 10 Hz pulse repetition, therefore 2000 mW equates to an average E_{pulse} of 200 mJ.

It is important to notice a limitation of our experiment as the chamber only has one window. Thanks to that a 0º mirror must be placed inside to reflect the laser beam and, as referenced before, the combustible mixture cannot be used. For the final combustion chamber, there is the possibility to perform a multi-pass laser absorption experiment since two pairs of facing optical ports exist in the design. Obviously such experiments require better windows, with a transmittivity higher than 99% in the characteristic wavelength of the laser radiation.

It is worth to notice that experimental uncertainty is large in the latter measurements. For $P_{in} \leq 800$ mW the used powermeter was no longer accurate to measure P_{out} due to being in the lower region of the scale, thus, data is inconsistent and must be ruled out. This is observable in Tab. 3.1, whose two last rows present experimental uncertainties relative to the measurement of 7 and 14 %, respectively. Not only this, but the powermeter scale was set to a maximum of 3000 mW, meaning that these measurements were taken from the lowest 10% of the scale, where most instruments are not very reliable. All the data was gathered and saved in similar manner to the one here presented.

Table 3.1: Laser power measurements for the He-O_2 mixture.

P_{in} (mW)	P_{out} (mW)
1950 ± 25	875 ± 25
1585 ± 25	700 ± 25
1200 ± 25	550 ± 25
810 ± 25	350 ± 25
400 ± 25	175 ± 25

Input and output laser power measurements for the He-O_2 mixture at 65.09 bar of filling pressure.

Errors and uncertainties propagation were treated using a linear approach, since no set of statistical data was collected, therefore only systematic errors/uncertainties and respective propagation were

[1] numbers represent each species molar fractions

considered. Linear error propagation theory states that for a parameter $F(a, b, c, ...)$ with uncertainty e_F, function of variables a, b, c whose uncertainties are e_a, e_b and e_c, respectively, its uncertainty is computed through the following equation:

$$e_F = \left|\frac{dF}{da}e_a\right| + \left|\frac{dF}{db}e_b\right| + \left|\frac{dF}{dc}e_c\right| = \sum_{i=1}^{n}\left|\frac{dF}{dx_i}e_{x_i}\right| \quad . \tag{3.1}$$

3.2 Minimum pulse energy to ignite H_2-air mixtures

In order to measure the influence of air:fuel equivalence ratio, pulse repetition and pulse energy in the ignition probability of H_2-air flows at atmospheric pressure, the following setup was assemble. Identically to the ESTHER experiments, this setup is also divided in two parts, an optical system and the combustion/burner as depicted in Fig. 3.3. When comparing it with the ESTHER experimental setup two major differences are presented, the gas is flowing rather than being stationary and its pressure is not up to 100 bar but atmospheric. This implies the need to focus the laser, otherwise ignition cannot be achieved due to its low pressure.

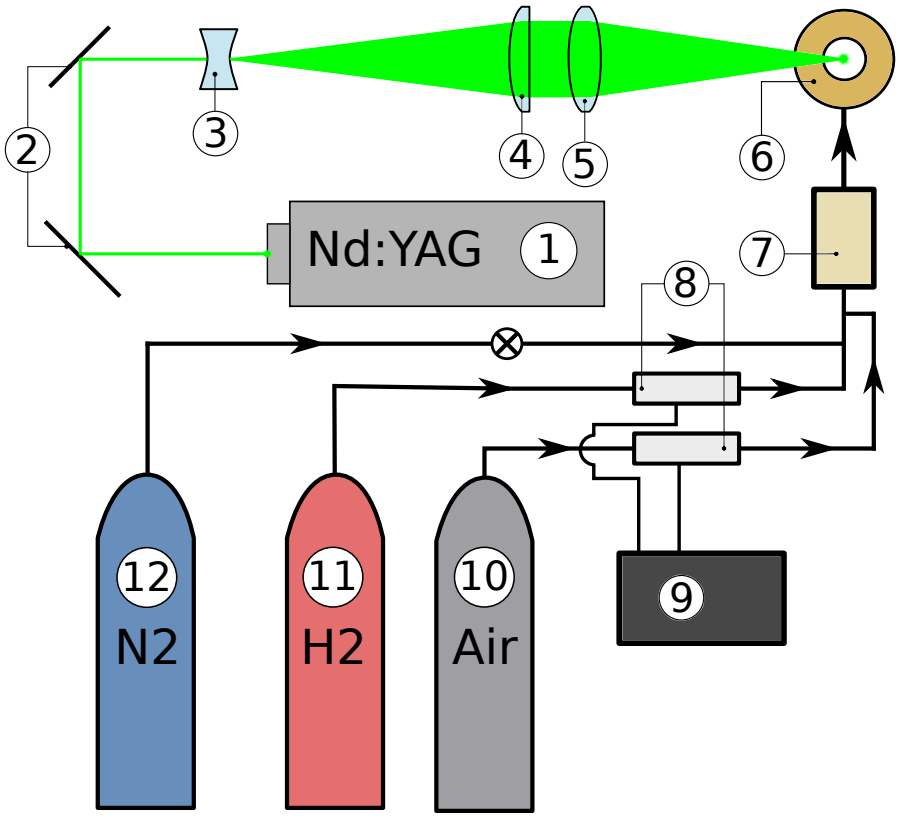

Figure 3.3: Schematic for H_2-air ignition experiment.

1 - Nd:YAG laser; 2 - 45º mirrors; 3 - bi-concave lens (f=-100 mm); 4 - plano-convex lens ($f = 700$ mm); 5 - bi-convex lens ($f = 100$ mm); 6 - Burner (10 mm diameter); 7 - Mixing box; 8 - Massflow controllers; 9 - Four-channel readout; 10-12 - Compressed gas bottles.

The optical system is composed of a Nd:YAG Laser (Litron Lasers Nano S 130-10, 1064 nm, 140 mJ, 6-8 ns, 2 mm radii, 10 Hz), two 45º mirrors (High power CVI Mirrors), one $f = -100$ mm, 1" diameter, bi-concave lens (Thorlabs), one $f = 700$ mm, 2" diameter, plano-convex lens (CVI) and one $f = 100$ mm, 2" diameter, bi-convex lens (Thorlabs). The laser beam is reflected in the two 45º mirrors and then expanded through the bi-concave and plano-convex lenses, a Galilean beam expander. A Galilean beam expander consists of a divergent lens (negative focal length) follow by a converging one (positive focal length), the distance between the lens d is parameterized by the equation $d = f_1 + f_2$, with f_1 and f_2 the lens's focal lengths. The magnification factor M is the factor for which the beam initial diameter is amplified, calculated as $M = -f_2/f_1$, for our setup M=7 and $d = 600$ mm. At last, the laser is focused using the bi-convex lens to a spot size given by Eq. (A.22). Using this lens setup a spark in air is formed centered with the burner axis and 1 cm above the top of it, which will ignite the combustible mixture. The hydrogen flow is provided by pressurized bottle (99% purity), while the air from an external compressor, both regulated and controlled with a set of mass flow controllers (MKS Instruments) and a four-channel readout (MKS Type 247D). The gases are mixed in a mixing box before passing through a flash arrestor, preventing the flame from burning backwards in accidental case. The gas flows at constant rate through the burner, and were tunned to be three to five times the burning velocity of H_2-air mixtures at 1 atm. This prevents the flame from burning into the burner, causing possible damage. This also makes an ease and prompt to operate experiment. Finally, a N_2 gas line is connected to the mixing box which is open in order to extinguish the burning flame. To calculate the different flows, $\dot{Q}$, the following set of equations were used:

$$\begin{aligned} \dot{Q}_{tot} &= \dot{Q}_{H_2} + \dot{Q}_{air} \quad , \\ \dot{Q}_{tot} &= A_{burn} v_{burn} \quad , \\ \phi &= 2.381 \times \frac{\dot{Q}_{H_2}}{\dot{Q}_{air}} \quad , \end{aligned} \tag{3.2}$$

where ϕ is the fuel:air equivalence ratio, defined as the reciprocal of λ, the air:fuel equivalence ratio, A_{burn} is the cross-section of the burner and v_{burn} is the burning velocity of mixture. One must notice that in pure H_2-O_2 burning the stoichiometric coefficients is 1/2, but air is formed of a mixture of 1 part of O_2 to 3.762 parts of N_2. Burning velocities for different ϕ were taken from [47]. The burner has 10 mm of diameter, thus A_{burn}=78.54 mm^2. Photographs of this experimental setup are shown in Appendix B.

Before the start, the mass flow controllers were turned on and warmed up during 1 hour. The air and H_2 flows were regulated so the total flow velocity equals four-times the burning velocity for a fixed value of ϕ. The laser was then warmed up for 15 minutes and set to fire in burst mode, meaning it will fire N pulses and then stop. The air flow was open, followed by the H_2 and wait 1 minute to homogenize the mixture, the laser was then fired and checked if ignition was or not achieved. This was done 10 times, and the number of successful ignitions registered. Next, the laser's energy output was altered by varying the Q-Switch delay time, between 150 and 500 μs, and the experiment ran again. Finally, the flow values were regulated to a different fuel:air equivalence ratio and the described procedure repeated.

Note that the laser energy for each Q-Switch delay was measured and calibrated. The laser's maximum energy output was 140.8$\pm$0.2 mJ. The results obtained with a powermeter (Coherent Fieldmax II) are presented in Tab. 3.2.

Table 3.2: Nd:YAG Laser pulse energy as function of the delay time of the Q-switch

Q-Switch delay (μs)	Energy fraction (%)	Pulse energy (mJ)
150	100	140.8$\pm$0.2
175	96.3 $\pm$ 1.1	135.7$\pm$1.7
200	88.8 $\pm$ 0.8	125.0$\pm$1.3
225	79.9 $\pm$ 0.5	112.5$\pm$0.8
250	73.1 $\pm$ 0.4	103.0$\pm$0.8
275	64.7 $\pm$ 0.4	91.0$\pm$0.7
300	53.4 $\pm$ 0.3	75.2$\pm$0.6
325	39.9 $\pm$ 0.3	56.2$\pm$0.4
350	30.5 $\pm$ 0.2	43.0$\pm$0.3
375	21.9 $\pm$ 0.2	30.8$\pm$0.3
400	13.7 $\pm$ 0.1	19.2$\pm$0.2

Chapter 4

Results & Discussion

4.1 Laser absorption at high pressure in ESTHER

Figures 4.1 and 4.2 show the overall transmittance of the optical system measured for He-O_2 and He-H_2 with partial composition of [10:1] and [9:2], respectively. The transmittance remains constant, about 0.45, for all the gas mixture filling pressures and laser input power between 1200 and 1950 mW. No observable difference was detected when changing the gas mixture composition.

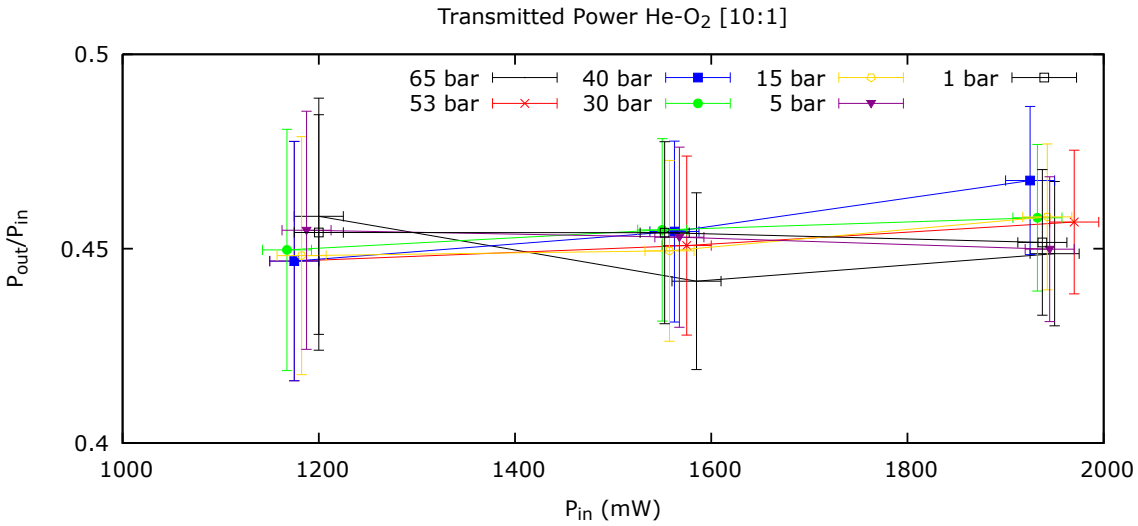

Figure 4.1: Transmittance as function of P_{in} and p for He-O_2 mixture.
Fraction of transmitted laser power, transmittance, function of input power P_{in} and filling pressure for a mixture of He-O_2 [10:1].

If we re-plot the data for He-H_2 [9:2] mixture at 100 bar of filling pressure we obtain Fig. 4.3. Clearly not only transmitted power fraction decreases for lower input powers as the experimental error increases as well. This figure supports what was already discussed in the reasoning to rule out the data points whose $P_{in} \leq 800$ mW. Not only the experimental absolute and relative errors increase significantly, leading to unreliable data as the data itself becomes incompatible with the theoretical law and incompatible

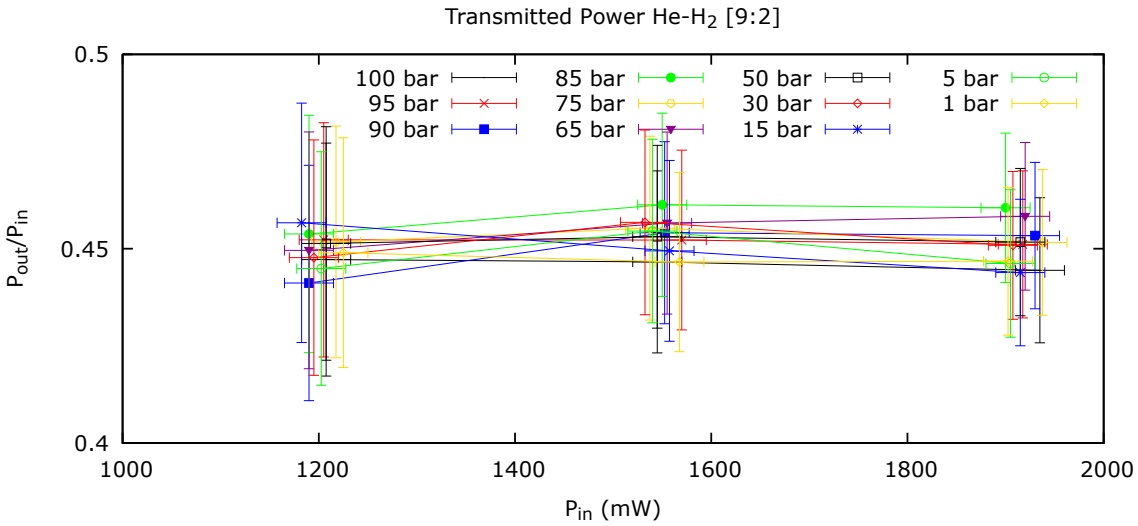

Figure 4.2: Transmittance as function of P_{in} and p for He-H_2 mixture.

Fraction of transmitted laser power, transmittance, function of input power P_{in} and filling pressure for a mixture of He-H_2 [9:2].

with several other laser absorption experiments.

Recalling Eq. (2.8), Beer-Lambert's law, the ratio $P(x)/P_0$ for a fixed position x is only function of the parameter α. This parameter is itself function of the medium on which the laser interacts and not of the laser itself, therefore is independent of P_0. In order to change α, the medium has to change, either becoming ionized by the laser or becoming saturated due to highly absorbed laser energy. Since neither of this nor others scenarios were observed, one can conclude that $d\alpha/dP_0 = 0$ for the current laser and gas parameters. In order to understand how the transmittance (and absorption) are function of the filling pressure, we took the average value for transmittance for fixed pressure, presented in Tab. 4.1 and depicted in Fig. 4.4.

Table 4.1: Average transmittance for different filling pressures

p (bar)	$\mathcal{T}_{He-H2}$	p (bar)	$\mathcal{T}_{He-O2}$
100.8 $\pm$ 0.2	0.4461 $\pm$ 0.0240	65.1 $\pm$ 0.2	0.4496 $\pm$ 0.0239
95.2 $\pm$ 0.2	0.4519 $\pm$ 0.0241	53.2 $\pm$ 0.2	0.4515 $\pm$ 0.0241
90.0 $\pm$ 0.2	0.4496 $\pm$ 0.0242	40.1 $\pm$ 0.2	0.4562 $\pm$ 0.0244
84.9 $\pm$ 0.2	0.4585 $\pm$ 0.0244	30.0 $\pm$ 0.2	0.4542 $\pm$ 0.0245
74.5 $\pm$ 0.2	0.4529 $\pm$ 0.0241	15.1 $\pm$ 0.2	0.4519 $\pm$ 0.0242
65.0 $\pm$ 0.2	0.4548 $\pm$ 0.0243	5.0 $\pm$ 0.2	0.4525 $\pm$ 0.0241
49.1 $\pm$ 0.2	0.4520 $\pm$ 0.0242	1.0 $\pm$ 0.2	0.4533 $\pm$ 0.0241
29.6 $\pm$ 0.2	0.4518 $\pm$ 0.0244		
15.1 $\pm$ 0.2	0.4500 $\pm$ 0.0243		
4.9 $\pm$ 0.2	0.4485 $\pm$ 0.0242		
1.0 $\pm$ 0.2	0.4474 $\pm$ 0.0239		

Average transmittance for laser absorption at different filling pressures, for both He-H_2 [9:2] (left side) and He-O_2 [10:1] (right side) mixtures.

One can notice from Fig. 4.4 that the average transmittance over P_{in} remains nearly constant with the pressure. This observation implies that despite the density being 100 times higher in the beginning

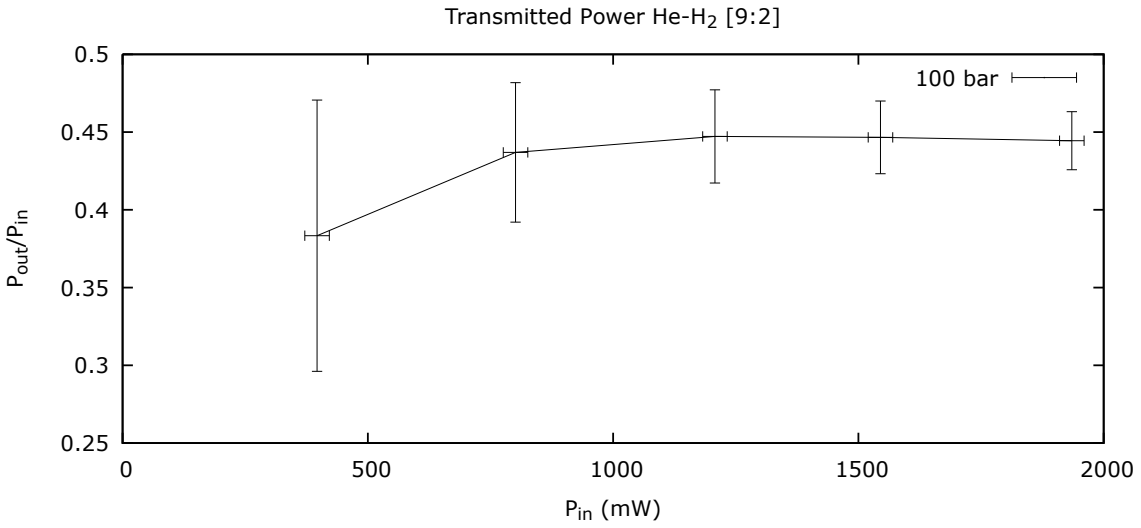

Figure 4.3: Transmittance as function of P_{in} and p for He-H_2 mixture, no filtered data.

Fraction of transmitted laser power, transmittance, function of input power P_{in} and filling pressure for a mixture of He-H_2 [9:2], no filtered data.

of the experiment comparing to the end, the fraction of energy absorbed by the gas, since all remaining mediums (silica window, mirror and optical distances) are set constant, is about the same.

The total transmittance $\mathcal{T}$ can be written as follows,

$$\mathcal{T}(p) = \mathcal{T}^2_{gas}(p) \times \mathcal{T}^2_{air} \times \mathcal{T}^2_{window} \times \mathcal{T}_{mirror} = \mathcal{T}_{opt}\mathcal{T}^2_{gas}(p) \quad , \tag{4.1}$$

where $\mathcal{T}_{gas}$, $\mathcal{T}_{air}$, $\mathcal{T}_{window}$ and $\mathcal{T}_{mirror}$ represent the partial transmittances of the chamber's gas mixture, air between powermeter and laser output, silica window and 0º mirror, respectively. The optical system transmittance is coupled into the $\mathcal{T}_{opt}$ term of Eq. (4.1). A squared term means two passes through, like the silica window, which is crossed twice by the laser beam. The gas filling system does not allow sub-atmospheric pressures inside the chamber, so the minimal achievable pressure was the atmospheric pressure p_0. In order to be possible to compute the gas transmittance $\mathcal{T}_{gas}$, a normalization was performed to the transmittance $\mathcal{T}(p_0)$. Separating the gas transmittance, $\mathcal{T}^2_{gas}(p) = \mathcal{T}^2_{gas}(\Delta p) \times \mathcal{T}^2_{gas}(p_0)$, where Δp is the excess pressure in relation to the atmospheric and coupling $\mathcal{T}_{gas}(p_0)$ with the optics part, $\mathcal{T}_{opt}$, we get:

$$\mathcal{T}(p) = \mathcal{T}_{opt} \times \mathcal{T}^2_{gas}(p_0) \times \mathcal{T}^2_{gas}(\Delta p) = \mathcal{T}_{p_0+opt} \times \mathcal{T}^2_{gas}(\Delta p) \quad . \tag{4.2}$$

Taking the data from Tab. 4.1, solving Eq. (4.2) in order to $\mathcal{T}_{gas}(\Delta p)$ and plot it, we get the gas transmittance as shown in Fig. 4.5.

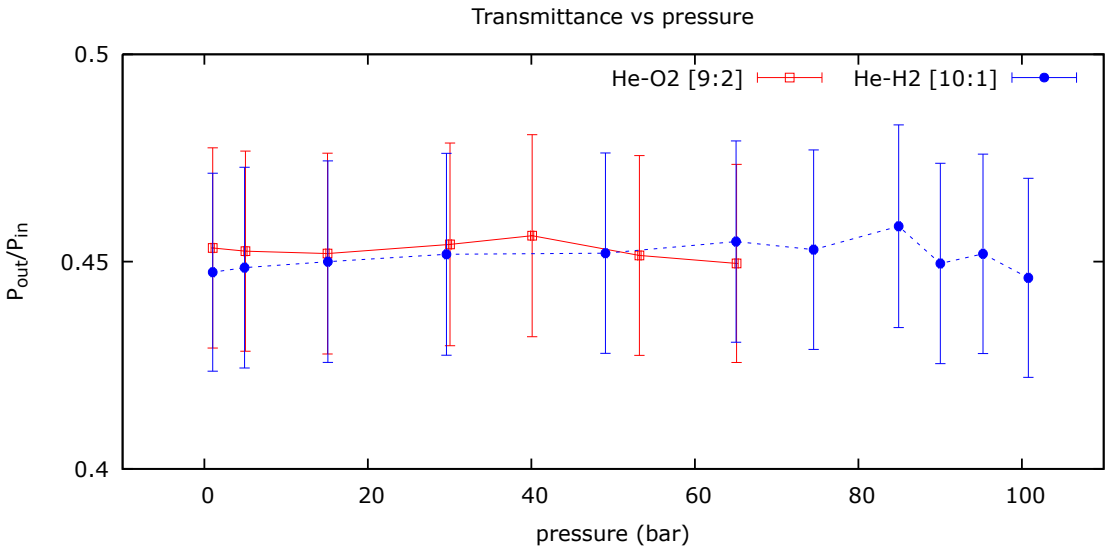

Figure 4.4: Average transmittance for both mixtures function of filling pressure

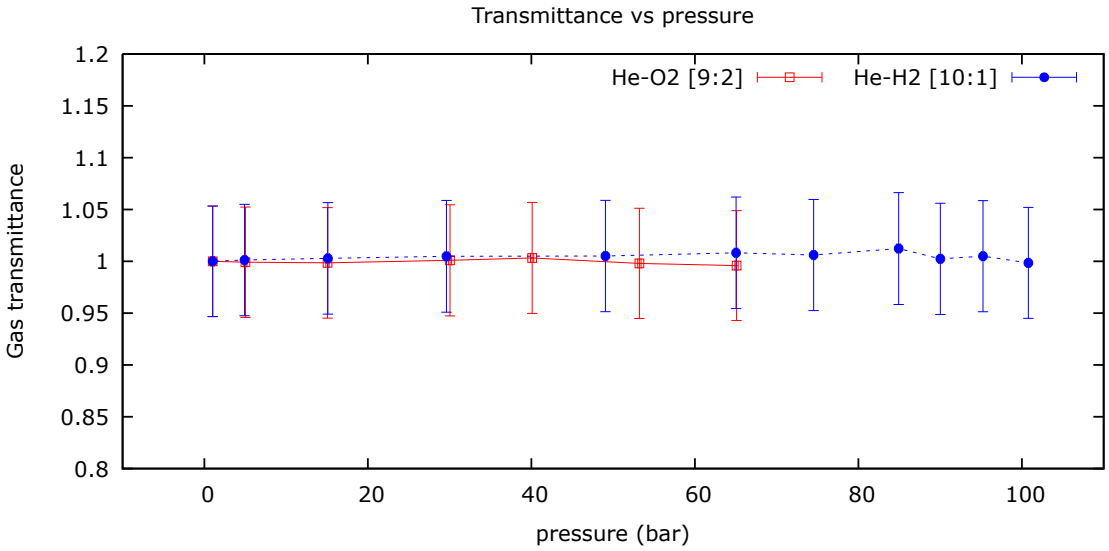

Figure 4.5: Gas transmittance for both mixtures as function of filling pressure[1]

[1] Note that the error propagation analysis leads to error bars with transmittance above 1. This obviously has no physical bearing.

The transmittance of the gas mixtures is constant and about 1, meaning the laser energy absorption is nearly 0 for this laser's wavelength. This observation was expected as the laser's wavelength was not tuned for the absorption wavelength of the mixture composing gases. To confirm this reasoning we can expand α as product of pressure p (a macroscopic parameter) and the absorption length density β (a microscopic parameter). Separating the gas absorption from the optical part (windows, mirrors), as before, we get from the Beer-Lambert's law:

$$\mathcal{T}(p) = \frac{P(x)}{P_0} = \exp(-\alpha l) = \exp(-\alpha_{gas} l_{gas}) \exp(-\alpha_{opt} l_{opt}) = \exp(-p\beta l_{gas}) \exp(-\alpha_{opt} l_{opt}) \quad . \tag{4.3}$$

Separating the total pressure p in atmospheric pressure, p_0 (≈1 bar) and excess pressure Δp, so $p = p_0 + \Delta p$, we get from Eq. (4.3):

$$\exp(-p\beta l_{gas}) = \exp(-(p_0 + \Delta p)\beta l_{gas}) \quad . \tag{4.4}$$

Since the total transmittances for Δp=0 and $\Delta p \neq$0 bar are similar, we can equate them,

$$\exp(-\alpha_{opt} l_{opt}) \exp(-p_0 \beta l_{gas}) \approx \exp(-\alpha_{opt} l_{opt}) \exp(-(p_0 + \Delta p)\beta l_{gas}) \quad . \tag{4.5}$$

Applying the $\ln$ function to both side of Eq. (4.5) we get:

$$\begin{aligned} -\alpha_{opt} l_{opt} - p_0 \beta l_{gas} &\approx -\alpha_{opt} l_{opt} - (p_0 + \Delta p)\beta l_{gas} \Rightarrow \\ p_0 \beta l_{gas} &\approx (p_0 + \Delta p)\beta l_{gas}. \end{aligned} \tag{4.6}$$

Since l_{gas} is constant and positive it can be simplified from Eq. (4.6), leading to:

$$p_0 \beta \approx (p_0 + \Delta p)\beta \quad , \tag{4.7}$$

which has two solutions, Δp=0 or β=0. Since Δp is neither zero nor negligible in comparison to p_0, the only solution is a β to be zero or very small, for which our experiment cannot detect the respective changes in the absorption coefficient α. This observation was expected as the laser's wavelength was not tuned for the absorption wavelength of the mixture composing gases. Another evidence to this conclusion is that both mixtures He-H_2 and He-O_2 transmission coefficients are, up to our precision, equal.

As expected, Fig. 4.5 presents a nearly constant value of transmittance about 1. This results means that the gas mixture is transparent to the laser light. As also observed in Fig. 4.4, no significant differences exist between the two gas mixtures and, for both of them, the gas transmittance is ≈1. This supports the idea that the laser's energy is absorbed initially by dust and other micro-particles, not the gas molecules, forming the seed electrons.

We have already reported that laser ignition was achieved in the ESTHER combustion chamber without focusing lens. This is a scientific breakthrough due to the irradiance being orders of magnitude lower than the ones presented in the literature, $\geq 10^{11}$ W/cm^2. The laser setup parameters used as ignition system in ESTHER combustion chamber are presented in Tab. 4.2, both laser spot area and optical transmittance for the silica window were measure, A_{beam}=23.15±0.43 mm^2 and $\mathcal{T}_{window}$=0.801, meaning I=1.336×10^8 W/cm^2.

Table 4.2: ESTHER laser ignition system parameters

E_{pulse} (mJ)	Δt_{pulse} (ns)	A_{beam} (mm^2)	$\mathcal{T}_{window}$	I (10^8 W/cm^2)
193 ± 2	5	23.15 ± 0.43	0.801	1.336 ± 0.039

Weinrotter et al. in [24] made ignition experiments up to 4 MPa (about 40 bar) of filling pressure

and reported a irradiance of 10^{11} W/cm^2, three orders of magnitude greater than our results. On this same reference the authors already hinted that first electrons are not generated through MPI, but by ionizing particles within the mixture. Our observation on the gas transmittance being pressure independent validates that dust and other particles are the ones which initially absorb the laser's energy. Whenever electrical breakdown occurs the laser's energy is absorbed by the plasma through inverse bremsstrahlung and transferred through pressure and heat to the unburned gas. The energy absorbed by the particles is low enough to not be detected by our setup, but can create a localized plasma hot enough to excite H_2 molecules around it and start the chemical chain reactions, leading to full scale ignition. Another observation was made, the initial silica window had several small points of damage on the inner face after 4 months and several combustion shots of use, hinting to being created as these micro particles are projected towards it when rapidly ionized by the laser.

4.2 Minimum pulse energy to ignite H_2-air mixtures

A first run of the experiment was performed with 10 pulse burst and ϕ between 0.3 and 5. Due to the precision of the massflow controllers, it is impossible to have the values of ϕ equal to the a priori chosen ones. In Tab 4.3 we present ϕ computed for the used experimental air and H_2 flows.

Table 4.3: Values for H_2 and air flows and corresponding fuel:air equivalence ratios

$\dot{Q}_{H_2}$(sccm)	$\dot{Q}_{air}$(sccm)	ϕ
6860 $\pm$ 20	1150 $\pm$ 10	0.399 $\pm$ 0.011
9610 $\pm$ 20	2020 $\pm$ 10	0.500 $\pm$ 0.008
13380 $\pm$ 30	3560 $\pm$ 10	0.634 $\pm$ 0.008
22500 $\pm$ 100	7560 $\pm$ 20	0.800 $\pm$ 0.014
26200 $\pm$ 100	9900 $\pm$ 20	0.900 $\pm$ 0.013
29600 $\pm$ 100	12460 $\pm$ 20	1.002 $\pm$ 0.012
32100 $\pm$ 100	15510 $\pm$ 20	1.150 $\pm$ 0.012
34500 $\pm$ 100	18760 $\pm$ 40	1.295 $\pm$ 0.016
34100 $\pm$ 100	21000 $\pm$ 1000	1.466 $\pm$ 0.176
33600 $\pm$ 100	23000 $\pm$ 1000	1.630 $\pm$ 0.180
32800 $\pm$ 100	25000 $\pm$ 1000	1.815 $\pm$ 0.186
31000 $\pm$ 100	26000 $\pm$ 1000	1.997 $\pm$ 0.198
28800 $\pm$ 100	27000 $\pm$ 1000	2.232 $\pm$ 0.215
27200 $\pm$ 100	27000 $\pm$ 1000	2.363 $\pm$ 0.229
24200 $\pm$ 100	26000 $\pm$ 1000	2.558 $\pm$ 0.259
20800 $\pm$ 100	25000 $\pm$ 1000	2.862 $\pm$ 0.305
18480 $\pm$ 30	24800 $\pm$ 100	3.195 $\pm$ 0.043
16090 $\pm$ 20	24000 $\pm$ 100	3.552 $\pm$ 0.046
13370 $\pm$ 20	22500 $\pm$ 100	4.007 $\pm$ 0.057
11260 $\pm$ 20	20900 $\pm$ 100	4.419 $\pm$ 0.069
8930 $\pm$ 20	18800 $\pm$ 100	5.013 $\pm$ 0.090

The optical system has an optical transmittivity of 92.68% (see the optical equations presented in Chapter 2) the irradiance is equal to 9.846 $\times 10^{14} E_{pulse}$ W/cm^2, with E_{pulse} in joules. Electrical breakdown was observed for E_{pulse} of 125 mJ or higher, meaning 1.233$\times 10^{14}$ W/cm^2, which is in agreement with the literature. For lower energies and different optical arrangements sparks could occur but not at every pulse. This supports the idea of seed electrons being created by ionization of dust and/or micro

particles. The ignition probability for a 10-burst pulse attempt is depicted in Fig. 4.6 as function of pulse energy and fuel:air equivalence ratio.

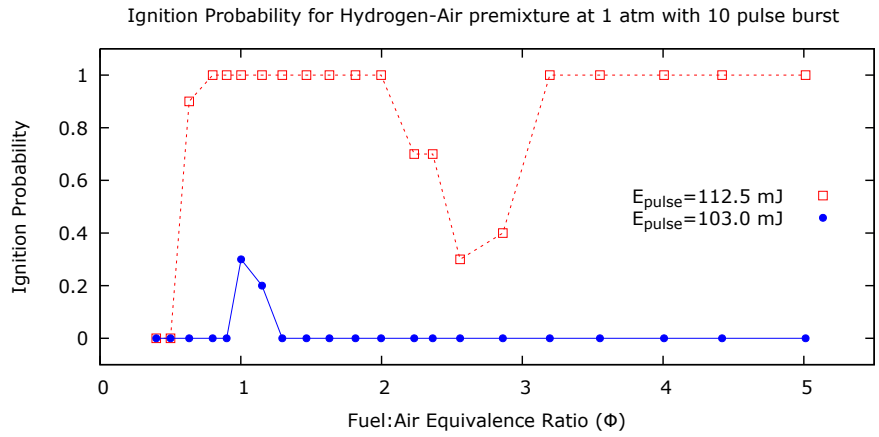

Figure 4.6: Ignition probability for H_2-air mixtures at 1 atm, 10-pulse burst and different ϕ and E_{pulse}.

In Fig. 4.6 we observe that for E_{pulse}=103 mJ the successful ignition in 10 attempts are 0 from ϕ=[0.4; 0.9], then it increases to 3 and 2 for ϕ=1 and 1.15, respectively. For $\phi \geq$1.3 and higher no successful ignition was achieved for this pulse energy. Also in Fig. 4.6 we show ignition probability for E_{pulse}=112.5 mJ, no ignition attempt is successful up to ϕ=0.65 with 9/10 successful ignitions. This probability then increases to 100% for ϕ=2.0, where it decreases to a minimum 3/10 at ϕ=2.65. Maximum probability is again reached at ϕ=3.2 staying there until ϕ=5.0.

Ignition was achieved using pulse energies smaller than the ones necessary to produce a visible spark and the rich side tends to be easier to ignite than the lean side. Both observations are in agreement with [24, 23, 22] whose observations report lower energies on the rich side comparing to the lean, with a minimum near the stoichiometric region. This is due to the formation of atomic excited highly reactive H-species, which is more difficult in the lean side. Notice that ϕ=0.4 or lower could not be ignited, despite being within hydrogen flammability limits and ignited with a lighter. One could also conclude that if the mixture is ignitable by a laser spark, by this means achieving a macroscopic spark in air ensures ignition, the reverse in not necessarily true.

It was expected, for a closed combustion vessel, that the minimum pulse energy to decreases up to stoichiometric region and then increases again. Our data does not reproduce this on the rich side of the mixture, presenting a decrease ignition probability after ϕ=2 but an increased ignition probability at ϕ=2.9. The reason for this can be relate to two phenomena, first minimum ignition energy increases far away from stoichiometric region, therefore pulse energy increases diminishing ignition probability. On the other hand, the region between ϕ=1.8 and 2.6 is characterized by high flow velocity which also increases the minimum ignition energy due to convective heat transfer on the flow, as in [40]. Another explanation for the non formation of a stable flame lies in the flame been blown out in the early stages of its formation. In the initial flame kernel the speed at which the energy and matter propagate outwards the kernel is slower than the burning velocity S_L. Since the mixture's flow velocity is four times S_L, the initial flame kernel could be blown out in a similar fashion to what occurs when the N_2 valve is

open and blows out the flame. On the far rich side the flow velocity is reduced again so the flame kernel can grow and stabilize before been blown out. The reasoning behind this explanation does not deny the occurrence of ignition itself, but nullifies the flame development related to the gas dynamics and heat/mass propagation. Two observations were made during this experimental run, the air sparks stopped after ignition and the ignition timing was variable for every 10-burst shot.

From the first observation one could conclude that no major electrical breakdown occurs in a burning flame. Since the particles around the flame are in various excitation states, some of them are even ionized as they absorb the laser energy in a smoother way. Without a sudden energy deposition no shockwave is generated, meaning no audible sound is produced (or heard). The second observation relates to the ignition probability with the electric breakdown. In some shots ignition was only achieved nearly by the 10th pulse, implying that the electrical breakdown did not occur until around the 10th pulse. This is in agreement with the seed electron theory and earlier observations of air spark formation without combustible mixture. Due to the breakdown mechanism being associated with a stochastic event, low-ionization energy particles being found in the lasers focal spot, not every pulse is capable of generating an electron cascade, thus creating an electrical breakdown and igniting the mixture. The randomness of this phenomena relates to different factors: energy and spot size fluctuations on each laser pulse, local concentration of hydrogen species (easier ignition is achieved for higher hydrogen concentrations), local presence of dust and other impurities to form seed electrons. In order to study how the number of pulses influence on the ignition probability, the experiment was ran now with a 5-pulse burst instead of a 10-pulse burst. These results are presented in Fig. 4.7.

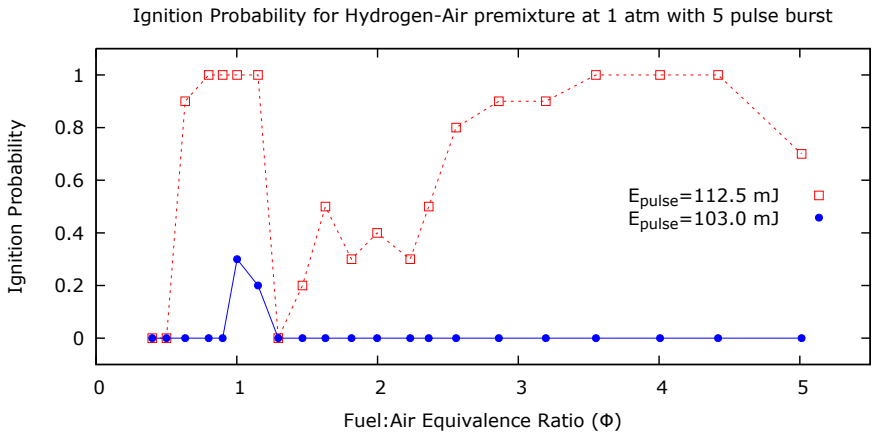

Figure 4.7: Ignition probability for H_2-air mixtures at 1 atm, 5 pulse burst and different ϕ and E_{pulse}.

In Fig. 4.7 we observe that for E_{pulse}=103 mJ the successful ignition in 10 attempts is 0 from ϕ=[0.4; 0.9], then it increases to 3/10 and 2/10 for ϕ=1 and 1.15, respectively. For $\phi \geq$1.3 no successful ignition was achieved for this pulse energy, 103 mJ. In Fig. 4.7 is also shown the ignition probability for E_{pulse}=112.5 mJ, where ignition is unsuccessful up to ϕ=0.65, there it rises to 9/10 successful ignitions. The ignition probability increases to 100% for ϕ=[0.8; 1.15], where after it abruptly decreases to a minimum of 0/10 at ϕ=1.3. The ignition probability starts to increase again in a non monotonous way, reaching a maximum probability at $\phi = 3.55$, presenting a decrease for $\phi = 5.0$ with 7/10 ignitions.

Comparing ignition with 10-and a 5-pulse burst, the general behaviour is similar in both regimes, with the 5-pulse regime having a lower success in igniting for ϕ between 1.30 and 3.20. Clearly, this is explained by the randomness of each laser pulse its interaction with the gas flow. As discussed before, spark formation is strongly related to the micro-particles presence in the air/mixture, which present a random/Brownian motion. For a pulse energy near the breakdown threshold, these fluctuations can be enough to hinder spark generation and therefore block ignition. One can also think of this as being a random event with a binomial distribution whose ignition probability is fixed between 0 a 1. After a sufficiently large number of events both results (ignition and non-ignition, in this case) will be present. Using 10-pulse burst increases the number of events and thus decreases the probability of every pulse lead to a non-ignition. Recurring to several pulses/ignition attempts for the same shot is not only a laser usual practice, as spark-plugs also recur to this technique to ensure ignition.

Chapter 5

Conclusions

5.1 Laser absorption at high pressure in ESTHER

As already stated, laser ignition was achieved in the ESTHER combustion chamber without focusing lens. This is a scientific novelty due to the irradiance being at least two orders of magnitude lower than the ones until now and to the extent of our knowledge, presented in the literature. The experiment of laser absorption at high pressures lead to the following conclusions:

a) The transmittance of a gas is independent of the input laser power - In agreement with previous experiments and theoretical models, the fraction of power transmitted through a optical medium is constant, up to our laser power. As the light passes through the medium it can interact with it, this probability being governed by the absorption coefficient α. Even using the maximum power of the laser, the gas medium did not change, therefore its absorption coefficient remained constant.

b) Transmittance is, up to our experimental precision, pressure independent - The main goal of this experiment was to study how the laser energy is absorbed by the gas at high pressures. Our results show that, up to our experimental precision, no significantly transmittance difference appears between low and high filling pressures. Despite varying the pressure between 1 and 100 bar, the transmittance was nearly constant.

c) The energy fraction absorbed by a gas for an untunned laser wavelength is less than 5% - As expected for an untunned laser wavelength the absorption coefficient α is small. The Nd:YAG laser used has a wavelength of 1064 nm, belonging to the Infrared region, in contrast most of absorption wavelengths for O_2, H_2 and He gases are in the ultraviolet region. Even at filling pressures of 100 bar no significant changes on transmittance were observed, meaning that no significant fraction of energy was absorbed by the gas. The experimental precision allow a conclusion that for an unfocused beam less than 5% of the laser's energy is absorbed by the gas.

d) Seed electrons needed for electrical breakdown are generated from the ionization of dust particles and not by multiphoton ionization process - Since the gas practically does not absorb the laser light, when electrical breakdown occurs the seed electrons (first generated electrons) must come from ionization of the volatile and solid particles, not the gas. In fact, direct gas ionization is through MPI process (and is nearly pressure independent). In contrast, several experiments, including ours, the gas breakdown or ignition presents an evident dependence on the filling pressure.

e) High pressure H_2-O_2-He gas mixtures can be ignited without a macroscopic spark using a unfocused laser beam - The ESTHER setup did not produce a visible or audible spark in the combustion chamber. When an electrical breakdown occurs a sharp sound is audible due to the pressure shock-wave, and this did not occur. Besides this, if an electrical spark would be generated the laser would be more absorbed, through the inverse bremsstrahlung process. We already reported ignition without a focused beam, and also we did not observe a macroscopic spark formation on a non-combustible mixture, which allows us to conclude that ignition can be achieve at high pressure without a macroscopic spark. Other experiments thought that a macroscopic spark was needed in order to ignite the combustible mixture, therefore the necessity of focusing the laser beam. A summary of the observables for different laser and mixture conditions are shown in Tab. 5.1.

Table 5.1: Observables for laser-induced spark ignition in high-pressure regime

	Non-Combustible mixture	Combustible mixture
Focused beam	Macroscopic spark	Macroscopic spark and ignition
Unfocused beam	—	Ignition

5.2 Minimum pulse energy to ignite H_2-air mixtures

Looking at the data and its processing the main conclusions driven from the study and experiment done at KAUST are:

a) Laser-induced spark ignition cannot ignite H_2-air mixture at the lean flammability limit - In agreement with previous experiments from different authors, a H_2-air mixture at the lean flammability limit could not be ignited through laser ignition. The observations made during the experiment shown that, even when using maximum pulse energy (140 mJ), ignition could not be achieved for $\phi \leq 0.5$. In spite of being able to ignited mixtures with $\phi \leq 0.5$ with a simple lighter, it acted as an effective lean flammability limit for laser ignition.

b) Laser ignition is more effective at the rich side of a combustible mixture - The rich side of H_2-air mixture proved to be relatively easier to ignite than the lean side. Ignition was achieved with ease, even at ϕ=5.0, which is closer to the theoretical rich flammability limit.

c) Minimum Pulse Energy decreases in the stoichiometric region - In agreement with other experiments, the stoichiometric and near-stoichiometric regions (ϕ=[1.0; 1.15]) achieved ignition for lower pulse energy, 103 mJ corresponding to a irradiance of 1.013 $\times 10^{14}$ W/cm^2. Ignition probability decreases as ϕ goes away from stoichiometric region, meaning a rise in the minimum pulse energy.

d) Increasing the mixture's flow velocity increases the minimum pulse energy - Ignition probability presents a sudden decrease in the region with ϕ between 2.20 and 3.20. This unexpected increase in minimum pulse energy (therefore in minimum ignition energy as well) can be related to an increase in flow velocity. One can justify the increase in MPE recalling that S_L has a maximum for ϕ=[2.20;3.20], which means heat convective losses increase as well. In the rich side, flow velocity decreases again, and the ignition probability therefore increases.

e) Producing a macroscopic spark in air guarantees ignition with limits - A macroscopic and visible air spark could be formed for E_{pulse}=125 mJ. If the mixture is within the effective flammability limits for laser-induced spark ignition, forming a macroscopic electric breakdown releases enough energy to excite the surrounding species and igniting the mixture. This is observable as the mixture ignite 10/10 times and without delay for pulse energy above the spark formation threshold.

f) Ignition is a probabilistic event, function of several parameters, such as pulse energy, air:fuel equivalence ratio, pressure - Laser-induced spark ignition is highly related to initial seed electrons originated from the ionization of micro-particles. The presence of sufficiently particles and H_2 species in the laser's focal region to produce a spark and excite the hydrogen, forming reactive radicals is an aleatory event. The data comparing 10-and 5-burst pulse supports this, since the 5-pulse burst clearly presents less successful ignitions than the 10-pulse burst for similar conditions.

5.3 Final remarks

The principal conclusions we can draw from both experimental setups and this work are: 1) laser ignition is a process highly influenced by the filling pressure of the chamber; 2) the laser's irradiance is the critical factor to determine if ignition is successful or not. At high pressures, above to 20 bar, ignition can be achieved without focusing a laser, reducing its irradiance to values lower than the macroscopic electrical breakdown threshold. This means macroscopic electrical sparks are not created for an unfocused laser, which agrees with the second experiment where ignition was achieved with E_{pulse} inferior to the electrical breakdown threshold. Ignition is achieved through the excitation of gas molecules, in a high pressure environment the particle density is sufficiently high so these can be excited by a smaller, even microscopic spark. This small spark is generated by the ionization of volatile particles in the mixture. Richer mixture are easier to ignite, supporting the idea that hydrogen species are critical in the start of chemical chain reactions. Since no macroscopic spark is needed to ignite, the actual ignition

region/point starts before and after the focal point, as shown in Fig. 5.1. Results from other authors [40, 22] already hinted towards this, as the spark was formed before the focal point.

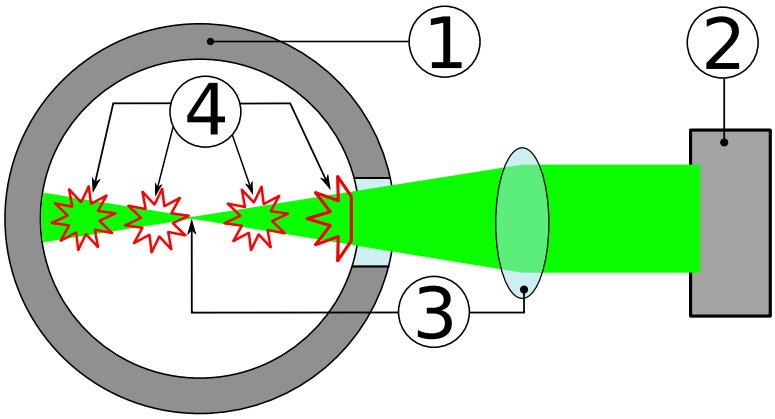

Figure 5.1: Illustration of a high pressure laser ignition.
1-Combustion Chamber; 2-Laser; 3-Focal lens and respective focal point; 4-Ignition region.

By chance, some interesting and completely unexpected events were caught during our research, since the current scientific literature did not even considered it as a possibility. Namely, the possibility of reaching ignition with a laser irradiance at least two orders of magnitude lower than expected or starting a flame without creating a macroscopic spark.

Further research is needed to understand why and in what conditions these events can take place. The first thing that comes to mind is the comparison of focused $vs.$ unfocused ignition.

Bibliography

[1] M. L. da Silva, B. B. de Carvalho, A. Smith, and L. Marraffa. High-pressure H_2/He/O_2 Combustion Experiments for the Design of the ESTHER Shock-tube Driver. In *46th AIAA Thermophysics Conference*, pages 2016–4156. AIAA AVIATION Forum, 2016.

[2] D. K. Srivastava, M. Weinrotter, K. Iskra, A. K. Agarwal, and E. Wintner. Characterisation of laser ignition in hydrogen–air mixtures in a combustion bomb. *International Journal of Hydrogen Energy*, 34(5):2475–2482, march 2009. doi:10.1016/j.ijhydene.2008.11.117.

[3] B. Lewis and G. von Elbe. *Combustion, Flames and Explosions of Gases*. Academic Press, 3rd edition, 1987.

[4] U. Maas and J. Warnatz. Ignition Processes in Hydrogen-Oxygen Mixtures. *Combustion and Flame*, 74(1):53–69, october 1988. doi: 10.1016/0010-2180(88)90086-7.

[5] P. D. Ronney. Laser versus conventional ignition of flames. *Optical Engineering*, 33(2):510–521, february 1994. doi: 10.1117/12.152237.

[6] D. R.Ballal and A. H.Lefebvre. The influence of flow parameters on minimum ignition energy and quenching distance. *Fifteenth Symposium on Combustion*, 15(1):1473–1481, 1975. doi:10.1016/S0082-0784(75)80405-X.

[7] B. Saleh and M. Teich. *Fundamentals of Photonics*. John Wiley & Sons, Inc, 1^{st} edition, 1991. Online ISBN: 9780471213741.

[8] P. Coelho and M. Costa. *Combustão*. Edições Orion, Lisboa, 2^{nd} edition, 2007. ISBN: 9789728620103.

[9] J. W. Heffel. NO_x emission reduction in a hydrogen fueled internal combustion engine at 3000 rpm using exhaust gas recirculation. *International Journal of Hydrogen Energy*, 39(11):293–601, november 2003. doi:10.1016/S0360-3199(02)00289-6.

[10] T. Shudoa, K. Omorib, and O. Hiyama. NO_x reduction and NO_2 emission characteristics in rich-lean combustion of hydrogen. *International Journal of Hydrogen Energy*, 33(17):4689–4693, september 2008. doi:10.1016/j.ijhydene.2008.05.034.

[11] W. M. Trott. CO_2-laser-induced deflagration of fuel/oxygen mixtures. *Journal of Applied Physics*, 54(1):118–130, september 1983. doi:10.1063/1.331737.

[12] B. Raffel, J. Warnatz, and J. Wolfrum. Experimental study of laser-induced thermal ignition in O_2/O_3 mixtures. *Applied Physics B*, 37(4):189–195, august 1985. doi:10.1007/BF00692940.

[13] U. Maasand, B. Raffel, J. Wolfrum, and J. Warnatz. Observation and simulation of laser induced ignition processes in O_2-O_3 and H_2-O_2 mixtures. *Twenty-First Symposium on Combustion*, 21(1): 1869–1876, august 1986. doi:10.1016/S0082-0784(88)80422-3.

[14] D. Lucas, D. Dunn-Rankin, K. Hom, and N. J. Brown. Ignition by excimer laser photolysis of ozone. *Combustion and Flame*, 69(2):171–184, august 1987. doi:10.1016/0010-2180(87)90029-0.

[15] M. Lavid and J. G. Stevens. Photochemical ignition of premixed hydrogenoxidizer mixtures with excimer lasers. *Combustion and Flame*, 60(2):195–202, may 1985. doi:10.1016/0010-2180(85)90007-0.

[16] M. Lavid, Y. Nachshon, S. K. Gulati, and J. G. Stevens. Photochemical Ignition of Premixed Hydrogen/Oxygen Mixtures with ArF laser. *Combustion Science and Tecnhology*, 96(4-6):231–245, may 1994. doi:10.1080/00102209408935357.

[17] B. E. Forch and A. W. Miziolek. Laser-based ignition of H_2O_2 and D_2O_2 premixed gases through resonant multiphoton excitation of H and D atoms near 243 nm. *Combustion and Flame*, 85(1-2): 254–262, may 1991. doi:10.1016/0010-2180(91)90192-E.

[18] B. E. Forch and A. W. Miziolek. Laser-based ignition of H_2O_2 and D_2O_2 premixed gases through resonant multiphoton excitation of H and D atoms: first report of deuterium isotope effect in laser ignition. In *27th JANNAF Combustion Meeting*, pages 219–227, 1990.

[19] R. G. Kingdon and F. J. Weinberg. The effect of plasma constitution on laser ignition energies. *Symposium (International) on Combustion*, 16(1):747–756, 1977. doi:10.1016/S0082-0784(77)80368-8.

[20] J. A. Syage, E. W. Fournier, R. Rianda, and R. B. Cohen. Dynamics of flame propagation using laser-induced spark initiation: Ignition energy measurements. *Journal of Applied Physics*, 64(3): 1499–1507, august 1988. doi:10.1063/1.341824.

[21] T. A. Spiglanin, A. Mcilroy, E. W. Fournier, R. B. Cohen, and J. A. Syage. Time-resolved imaging of flame kernels: Laser spark ignition of H_2/O_2/Ar mixtures. *Combustion and Flame*, 102(3):310–328, august 1995. doi:10.1016/0010-2180(94)00278-Z.

[22] T. X. Phuoc and F. P. White. Laser-Induced Spark Ignition of CH_4/Air mixtures. *Combustion and Flame*, 119(3):203–216, november 1999. doi: 10.1016/S0010-2180(99)00051-6.

[23] T. X. Phuoc. Laser-induced spark ignition fundamentals and applications. *Optics and Lasers in Engineering*, 44:351–397, June 2006. doi: 10.1016/j.optlaseng.2005.03.008.

[24] M. Weinrotter, H. Kopecek, E. Wintner, and M. Lackner. Application of laser ignition to hydrogen-air mixtures at high pressures. *International Journal of Hydrogen Energy*, 30:319–326, March 2005. doi: 10.1016/j.ijhydene.2004.03.040.

[25] J. Tauer, H. Kofler, K. Iskra, G. Tartar, and E. Wintner. Laser Plasma-initiated Ignition of Engines. In I. A. E. Agency, editor, *Proceedings of the 3rd International Conference on the Frontiers of Plasma Physics and Technology*, 2007.

[26] H. Kopecek, S. Charareh, M. Lackner, C. Forsich, F. Winter, J. Klausner, G. Herdin, and E. Wintner. Laser Ignition of Methane-Air Mixtures at High Pressures and Diagnostics. In *Proceedings of ICES03*, volume 614, pages 147–154. ASME, 2003. doi: 10.1115/ICES2003-0614.

[27] H. Kopecek, H. Maier, G. Reider, F. Winter, and E. Wintner. Laser ignition of methane-air mixtures at high pressures. *Experimental Thermal and Fluid Science*, 27(4):499–503, april 2003. doi: 10.1016/S0894-1777(02)00253-4.

[28] T. X. Phuoc. Laser spark ignition: experimental determination of laser-induced breakdown thresholds of combustion gases. *Optics Communications*, 175(4–6):419–423, march 2000. doi: 10.1016/S0030-4018(00)00488-0.

[29] T.-W. Lee, V. Jain, and S. Kozola. Measurements of Minimum Ignition Energy by Using Laser Sparks for Hydrocarbon Fuels in Air: Propane, Dodecane, and Jet-A Fuel. *Combustion and Flame*, 125(4):1320–1328, june 2001. doi: 10.1016/S0010-2180(01)00248-6.

[30] C. Grey-Morgan. Laser-induced breakdown of gases. *Reports on Progress in Physics*, 38(5): 621–665, 1975. doi:10.1088/0034-4885/38/5/002.

[31] G. Weyl. *Laser-induced plasmas and applications*. Marcel Dekker, 1989.

[32] T. Hughes. *Plasma and laser light*. Wiley, 1975.

[33] A. Gold and H. B. Bebb. Theory of Multiphoton Ionization. *Physics Review Letters*, 14(3):60–63, january 1965. doi:10.1103/PhysRevLett.14.60.

[34] Y. B. Zeldovic and Y. P. Raizer. Cascade Ionization of a gas by a light pulse. *Soviet Physics JETP*, 20(3), 1965.

[35] A. V. Phelps. *Theory of growth of ionization during breakdown*. McGraw-Hill, 1966.

[36] A. Dalgarno and N. Lane. Free-free transition of electrons in gases. *Astrophysical Journal*, 145: 623–633, august 1966. doi:10.1086/148801.

[37] N. Kroll and K. M. Watson. Theoretical Study of Ionization of Air by Intense Laser Pulses. *Physical Reviews A*, 5:1883–1905, april 1972. doi:10.1103/PhysRevA.5.1883.

[38] D. I. Rosen and G. Weyl. Laser-induced breakdown in nitrogen and the rare gaes at 0.53 and 0.35 μm. *Journal of Physics D: Applied Physics*, 20(10):1264, april 1987. doi:10.1103/PhysRevA.5.1883.

[39] C. H. Chan, C. D. Moody, and W. B. McKnight. Significant loss mechanisms in gas breakdown at 10.6 μ. *Journal of Applied Physics*, 44(3):1179–1188, march 1973. doi:10.1063/1.1662325.

[40] D. Bradley, C. Sheppard, I. Suardjaja, and R. Woolley. Fundamentals of high-energy spark ignition with lasers. *Combustion and Flame*, 138(1–2):55–77, May 2004. doi: 10.1016/j.combustflame.2004.04.002.

[41] R. G. Root. *Laser-induced plasmas and applications*. Dekker, 1989.

[42] J. X. Ma, D. R. Alexander, and D. E. Poulain. Laser Spark ignition and Combustion Characteristics of methane-air mixtures. *Combustion and Flame*, 112(4):492–502, march 1998. doi: 10.1016/S0010-2180(97)00138-7.

[43] G. I. Taylor. The formation of a blast wave by a very intense explosion i. theoretical discussion. *PRoceedings of the Royal Society A*, 201(1065), march 1950. doi:10.1098/rspa.1950.0049.

[44] K. Dharamshi, D. K. Srivastava, and A. K. Agarwal. Characterisation of laser ignition in hydrogen–air mixtures in a combustion bomb. *International Journal of Hydrogen Energy*, 39(1):293–601, january 2014. doi:10.1016/j.ijhydene.2013.10.045.

[45] X. Liu and Q. Zhang. Influence of initial pressure and temperature on flammability limits of hydrogen–air. *International Journal of Hydrogen Energy*, 39(12):6774–6782, april 2014. doi:10.1016/j.ijhydene.2014.02.001.

[46] T. X. Phuoc and F. P. White. An optical and spectroscopic study of laser-induced sparks to determine available ignition energy. *Proceedings of the Combustion Institute*, 29(2):1621–1628, 2002. doi:10.1016/S1540-7489(02)80199-7.

[47] M. Kuznetsov, S. Kobelt, J. Grune, and T. Jordana. Flammability limits and laminar flame speed of hydrogen/air mixtures at sub-atmospheric pressures. *International Journal of Hydrogen Energy*, 37 (22):17580–17588, november 2012. doi:10.1016/j.ijhydene.2012.05.049.

Appendix A

Theoretical Fundamentals

A.1 Laser interaction with matter

When a photon, light particle, goes through a medium it can interact with it. This behavior is governed by Quantum Electrodynamics, and so, it is a stochastic event. A photon may, or may not, be absorbed p.e. by the medium, and the probability of being absorbed is proportional to the number of photons the beam has. Considering a laser as the light source, its power P is function of the number of emitted photon, so when it interacts with a medium it follows

$$\frac{dP}{dx} = -\alpha(x)P \quad , \tag{A.1}$$

where α is the absorption coefficient, function of the medium, wavelength, and other variables and x the optical path direction. This is known as the Beer-Lambert law, whose effect was first discovered by Pierre Bouger in 1729. This equation can also be derived as a solution for BGK equation. If we consider the absorption coefficient to be constant, a reasonably approximation for most cases as wavelength is constant and the medium homogeneous. Therefore Eq. (A.1) can be integrated to,

$$P(x) = P_0 \times \exp(-\alpha x) \quad , \tag{A.2}$$

where P_0 is the initial radiative power of the light source. Since the energy must be conserved, this implies the power also is, thus, initial power must be equal to the sum of transmitted, reflected and absorbed power. This is conservation is expressed in Eq. (A.3),

$$P_0 = P_t + P_r + P_a \quad , \tag{A.3}$$

where the subscript t, r, a represents transmitted, reflected and absorbed fractions, respectively. The fraction of power transmitted through the medium is known as transmittance, $\mathcal{T}$ and defined as:

$$\mathcal{T} = \frac{P_t}{P_0} \quad . \tag{A.4}$$

Neglecting the reflected power, a good approximation as the equipment is designed for the Nd:YAG laser's wavelength of 1064 nm, therefore, $P_0 \approx P_t + P_a$. Recalling Eqs. (A.2), (A.4) and (A.3), the absorbed power by the medium is given by:

$$P_a = P_0 \times (1 - \exp(-\alpha x)) = P_0 \times (1 - trans) \quad . \tag{A.5}$$

A.2 Laser mathematical properties

The propagation of electromagnetic waves in vacuum is governed by the so-called wave equation. First derived by d'Alembert in 1746 for an one dimension wave propagation, and then generalized by Euler for a three-dimension (x, y, z) movement. For an electromagnetic wave u propagating at a velocity c the equation reads,

$$\frac{\partial^2 u}{\partial^2 x} + \frac{\partial^2 u}{\partial^2 y} + \frac{\partial^2 u}{\partial^2 z} - \frac{1}{c^2}\frac{\partial^2 u}{\partial^2 t} = \nabla^2 u - \frac{1}{c^2}\frac{\partial^2 u}{\partial^2 t} = 0 \quad . \tag{A.6}$$

For a monochromatic wave such as a laser beam the time dependence can be described by an harmonic oscillator, and considering the spatial part $(x, y, z) = \mathbf{r}$ to simplify the notation, u holds,

$$u(\mathbf{r}, t) = a(\mathbf{r}) \cos(2\pi\nu t + \phi(\mathbf{r})) = a(\mathbf{r}) \cos(\omega t + \phi(\mathbf{r})) \quad , \tag{A.7}$$

where a is the amplitude of the wave, ν the frequency and ϕ a phase. The frequency of oscillation relates to the natural wavelength of the laser λ_0 by $c = \lambda_0 \times \nu$. One can, for convenience, define u as the real part of a complex quantity U, such that following equations hold true:

$$\begin{aligned} U(\mathbf{r}, t) &= a(r) \exp(i\phi(\mathbf{r})) \exp(i\omega t) = u(\mathbf{r}) \exp(i\omega t) \\ u(\mathbf{r}, t) &= Re\{U(\mathbf{r}, t)\} = \frac{1}{2}\{U(\mathbf{r}, t) + U^*(\mathbf{r}, t)\} \quad . \end{aligned} \tag{A.8}$$

If we replace U in the wave equation, Eq. (A.6), it still holds true. As time dependence is now explicit in the solution, it can be remove to obtain the Helmholtz equation:

$$\nabla^2 U + k^2 U + 0 \quad , k = \frac{2\pi\nu}{c} = \frac{\omega}{c} \quad . \tag{A.9}$$

The k parameter is the wavenumber, the angular equivalent to the wavelength. In a physical system such as electromagnetic waves, u is the Electric field, and the optical intensity (or irradiance) $I(\mathbf{r})$ is defined as $I(\mathbf{r}) = 2\left\langle u^2(\mathbf{r}, t)\right\rangle$. Using the complex expression for a monochromatic wave and averaging over a period $(1/\nu)$, we get $I = |U(\mathbf{r})|^2$.

The most simple solution for the Helmholtz equation is the plane wave, $U(\mathbf{r}) = A \exp(-i\mathbf{k} \cdot \mathbf{r})$. This solution has constant amplitude and propagates in the direction of the wavevector **k**. It is important to define what is a wavefront. Wavefronts are the surfaces of equal phase, $\phi(\mathbf{r}) = 2\pi q$ $(q = 1, 2, ...)$. At a given position **r** one can defined a normal vector parallel to its gradient vector, namely the wavefront

normal. In reality plane waves do not exist, a much more useful and physical wave is the paraxial wave. A paraxial wave propagates as a plane wave, (let's say in the z-direction) but, its complex amplitude is modulated as an slowly varying envelope such as:

$$U(\mathbf{r}) = A(\mathbf{r})\exp(-ikz) = |A(\mathbf{r})|e^{iarg(A(\mathbf{r}))}\exp(-ikz) \quad . \tag{A.10}$$

A paraxial wave's amplitude varies slowly along a wavelength, which is mathematically represent by $\partial A/\partial z \ll A/\lambda$. Expanding the Helmholtz equatio, Eq. (A.9) leads to the paraxial Helmholtz equation,

$$\begin{aligned} \nabla^2 A + k^2 A &= \frac{\partial^2 A}{\partial^2 x} + \frac{\partial^2 A}{\partial^2 y} - i2k\frac{\partial A}{\partial z} + \frac{\partial^2 A}{\partial z} \\ &\approx \frac{\partial^2 A}{\partial^2 x} + \frac{\partial^2 A}{\partial^2 y} - i2k\frac{\partial A}{\partial z} \\ &= \nabla_\perp^2 A - i2k\frac{\delta A}{\delta z} = 0 \quad , \end{aligned} \tag{A.11}$$

where $\nabla_\perp^2$ is the laplacian is the direction perpendicular to the beam's direction. One of the solutions for the paraxial Helmholtz equation is the Gaussian beam.

A.3 Gaussian beam

A paraxial wave has wavefronts whose normals are paraxial rays, its complex amplitude $U(\mathbf{r})$ satisfies Helmholtz equation and $A(\mathbf{r})$ the paraxial Helmholtz equation as well. A paraxial wave is equivalent to the approximation of a infinite cylindrical wire in electrodynamics where one direction is privileged over the other two. A important solution is the Gaussian beam whose amplitude $A(\mathbf{r})$ follows,

$$\begin{aligned} A(\mathbf{r}) &\approx \frac{A_1}{q(z)}\exp\left[-ik\frac{\rho^2}{2q(z)}\right] \\ \rho^2 = x^2 + y^2 \, , q(z) &= z + iz_0 \quad , \end{aligned} \tag{A.12}$$

where $q(z)$ is the beam's parameter and ρ is the radial direction as defined. For convenience $q(z)$ can be written as:

$$\frac{1}{q(z)} = \frac{1}{z + iz_0} = \frac{1}{R(z)} - i\frac{\lambda_0}{\pi w^2(z)} \quad . \tag{A.13}$$

On the definition of $q(z)$, z_0 is the Rayleigh range and z the distance to the beam's waist (which will be defined ahead). Recalling $U(\mathbf{r}) = A(\mathbf{r})e^{-ikz}$, the complex amplitude of the Gaussian beam is given by,

$$
\begin{aligned}
&U(r) = A_0 \frac{w_0}{w(z)} \exp\left[-\frac{\rho^2}{w^2(z)}\right] \exp\left[-i(kz - \zeta(z))\right] \exp\left[-ik\frac{\rho^2}{2R(z)}\right] \quad \text{with,} \\
&A_0 = \frac{A_1}{iz_0} \quad , \\
&w(z) = w_0\sqrt{1 + \left(\frac{z}{z_0}\right)^2} \quad , \\
&w_0 = \sqrt{\frac{\lambda_0 z_0}{\pi}} \quad , \\
&R(z) = z\left[1 + \left(\frac{z}{z_0}\right)^2\right] \quad , \\
&\zeta(z) = \arctan(z/z_0) \quad .
\end{aligned}
\tag{A.14}
$$

The beam is fully characterized by A_0, z_0 and λ_0. The first exponential and fraction describe the beam spread, the second one the phase delay relative to a plane or spherical wave, and the last the phase shift due to measuring a spherical surface along a plane. The irradiance for a Gaussian beam can be computed as follows,

$$
I(\rho, z) = |U(\mathbf{r})|^2 = I_0\left[\frac{w_0}{w(z)}\right]^2 \exp\left[-\frac{2\rho^2}{w^2(z)}\right] \quad , I_0 = |A_0|^2 \quad . \tag{A.15}
$$

It is trivial to conclude that maximum intensity is at the beam's axis ($\rho = 0$), and decreases monotonically with increasing ρ. The beam width is given by the function $w(z)$, and one can see that has a minimum, w_0, for $z = 0$. The radii for the wavefronts are given by $R(z)$ function, it is important to notice that $R(0) = \infty$, meaning the wavefront is a plane wave. Recalling the definition of $q(z)$, one can know fully understand that it relates the beam's natural characteristics waist w_0 and wavelength λ_0 to the axial distance z. At $z = 0$ the beam is most focus and defined, since its diameter ($2w_0$) is minimum. The beam's divergence θ evaluates the beam's spread over distance. For large z and recalling Eq. (A.14) we get,

$$
w(z) = w_0\sqrt{1 + \left(\frac{z}{z_0}\right)^2} \approx \frac{w_0}{z_0} z \quad , \theta = \frac{\lambda_0}{\pi w_0} \quad . \tag{A.16}
$$

The divergence angle is then defined as $2\theta = \frac{4}{\pi}\frac{\lambda_0}{2W_0}$. To calculate the power $P(z)$, we integrate the irradiance over the its area A as follows,

$$
P(z) = \int_A I(\rho, z) dA = \int_0^\infty I(\rho, z) 2\pi\rho d\rho = \frac{\pi}{2} I_0 W_0^2 \quad . \tag{A.17}
$$

From Eq. (A.17) is important to notice that total power equals the product of beam's area with half of the peak intensity and, it is independent of z, which verifies energy conservation.

Now that the amplitude factor of U is fully defined, we will look on to the phase, the second and third terms in Eq. (A.14). First lets denote the imaginary phase $\phi(\rho, z)$ as

$$\phi(\rho, z) = [kz - \zeta(z)] + k\frac{\rho^2}{2R(z)} \quad . \tag{A.18}$$

The first term kz is the phase of a simple plane wave propagating along z. The second one is called Gouy effect and is specific for the Gaussian beam as differentiates it from either a plane or a spherical wave. The last term is responsible for the wavefront bending as it shifts from a plane to a spherical wavefront.

A.4 Optics

A usual optical system has various optic devices such as mirrors, different lenses, fiber optics, polarizers, among others. The ABCD matrices are a powerful tool for computation on ray optics, but can still be used in Gaussian beams. The formalism is only valid on the paraxial approximation, for which $\sin x \approx x$, such as a Gaussian beam. Consider a ray that before entering an optical system has at height y_1 and making an angle θ_1 with the horizontal direction and after at height y_2 and angle θ_2. An optical system can be represented by a ABDC matrix such that it verifies the relation

$$\begin{bmatrix} y_2 \\ \theta_2 \end{bmatrix} = \begin{bmatrix} \mathrm{A} & \mathrm{B} \\ \mathrm{C} & \mathrm{D} \end{bmatrix} \begin{bmatrix} y_1 \\ \theta_1 \end{bmatrix} \tag{A.19}$$

In an optical system with n elements the ABCD matrix for the total system is the matrix product of its element's ABCD matrices ($\mathbf{M}_i$). The order of the matrices is the inverse order of the rays's optic path, as it follows,

$$\begin{bmatrix} y_n \\ \theta_n \end{bmatrix} = \mathbf{M}_n \mathbf{M}_{n-1} ... \mathbf{M}_2 \mathbf{M}_1 \begin{bmatrix} y_1 \\ \theta_1 \end{bmatrix} \tag{A.20}$$

Despite its limitations ABCD matrices are usual for the majority of optical systems. The ABCD matrices for the most common optical elements are depicted in Table A.1.

When considering a Gaussian beam, one important note regarding ABCD matrices needs to be done, since the q parameter does not appear directly in the formalism. Since q relates to the beam's waist and Rayleigh range to fully define the beam's characteristic it must also relates to the optical system. The relation between q-parameter before and after the optical system, q_1 and q_2, respectably, is given by the ABCD law, in Eq. A.21,

$$q_2 = \frac{\mathrm{A}q_1 + \mathrm{B}}{\mathrm{C}q_1 + \mathrm{D}} \quad . \tag{A.21}$$

It can be conclude from the ABCD law and the relations between q and w_0 that the beam's waist, w_2, at the focal distance, f, from an initial waist w_1 is given by:

$$w_2 = \frac{\lambda_0 f}{\pi w_1} \quad . \tag{A.22}$$

Table A.1: Table with ABCD matrices for different optical elements

Optical Element	ABCD Matrix	Remarks
Propagation in free space or in a medium of constant refractive index	$\begin{bmatrix} 1 & d \\ 0 & 1 \end{bmatrix}$	d = distance
Refraction at a flat interface	$\begin{bmatrix} 1 & 0 \\ 0 & \frac{n_1}{n_2} \end{bmatrix}$	n_1 = initial refractive index n_2 = finial refractive index
Reflection from a flat mirror	$\begin{bmatrix} 1 & 0 \\ 0 & 1 \end{bmatrix}$	Only valid for mirrors perpendicular to the propagation direction
Thin lens	$\begin{bmatrix} 1 & 0 \\ \frac{-1}{f} & 1 \end{bmatrix}$	f = lens focal distance Valid for $f \gg$ lens's thickness

Appendix B

Experimental Setup Photos

B.1 Laser absorption at high pressures in ESTHER

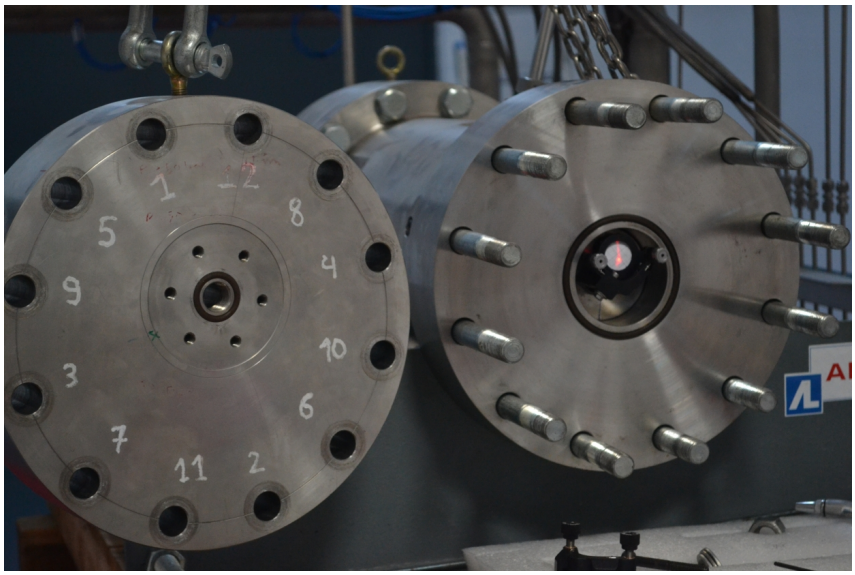

Figure B.1: Laser absorption combustion chamber and 0º mirror.

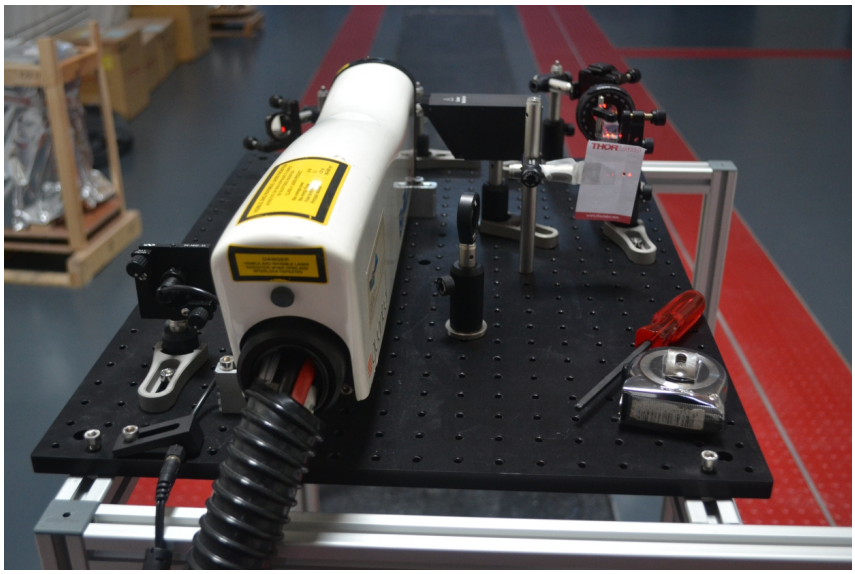

Figure B.2: Laser absorption experiment optical setup.

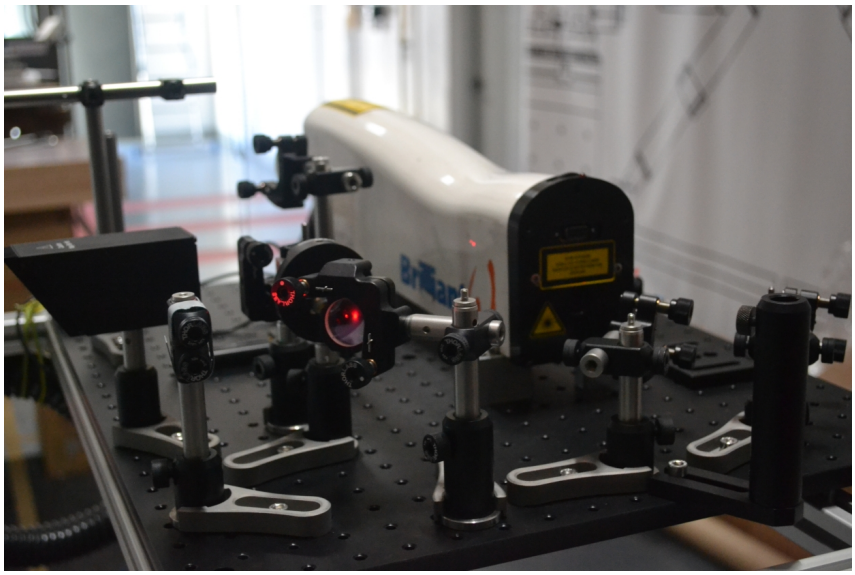

Figure B.3: Laser absorption experiment optical setup in detail.

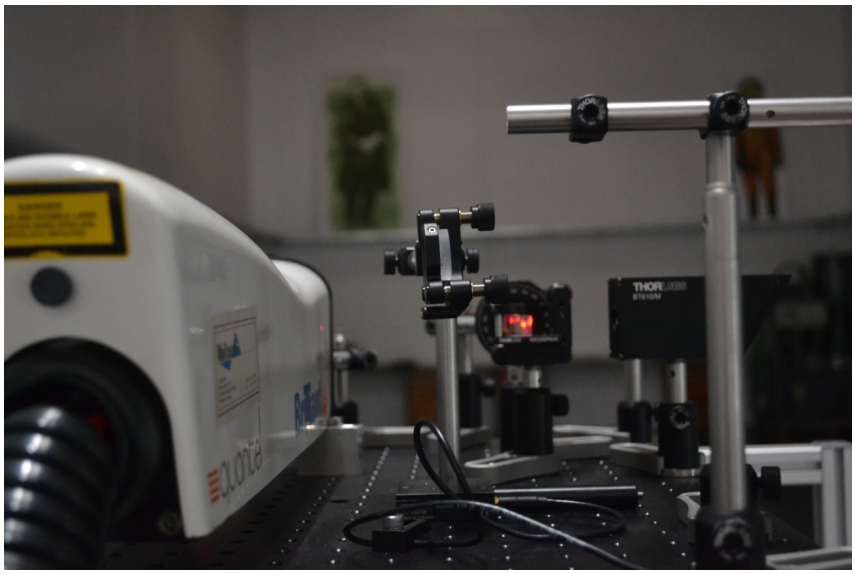

Figure B.4: Laser absorption experiment optical setup in detail.

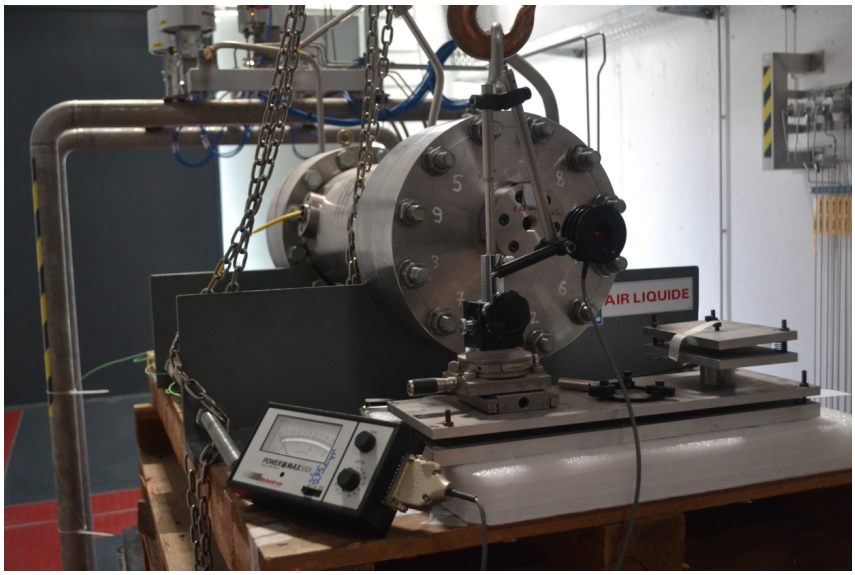

Figure B.5: Laser absorption experiment power measurement.

B.2 Minimum pulse energy for ignition of H_2-Air flows

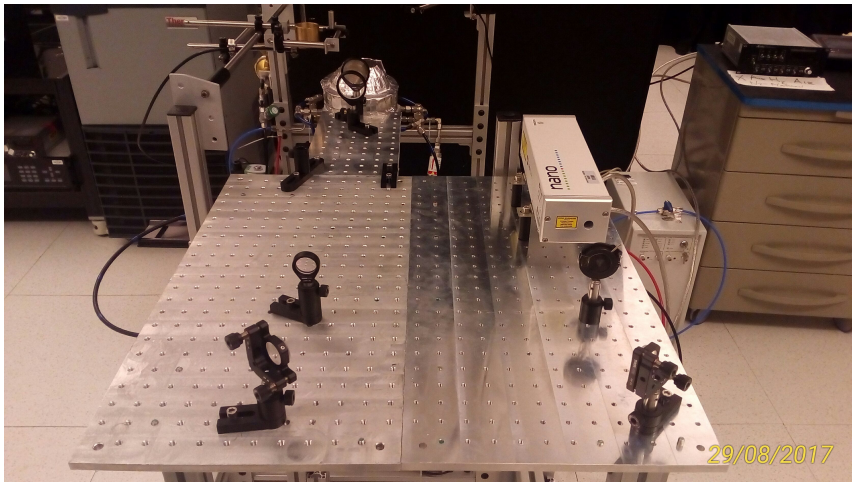

Figure B.6: Laser ignition experiment optical setup.

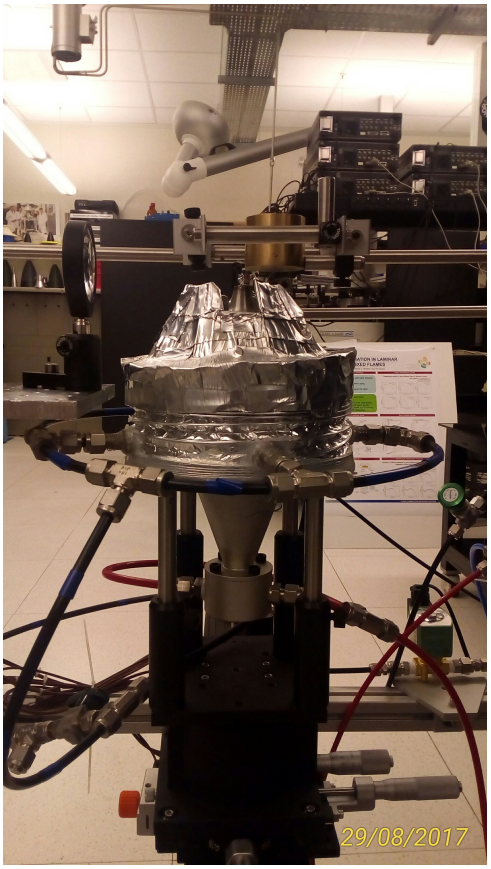

Figure B.7: Laser ignition experiment burner.